Oil & Gas Science and Technology – Rev. IFP Energies nouvelles **76**, 5 (2021)
© R. Prada Silvy & S.K. Lageshetty, published by IFP Energies nouvelles, 2020
https://doi.org/10.2516/ogst/2020084

Available online at:
ogst.ifpenergiesnouvelles.fr

REGULAR ARTICLE OPEN ACCESS

Conversion of heavy gasoil into ultra-low sulfur and aromatic diesel over NiWRu/TiO_2–γAl_2O_3 catalysts: Role of titanium and ruthenium on improving catalytic activity

Ricardo Prada Silvy* and Sathish Kumar Lageshetty

Applied Science & Technology Consulting, 4312 Blue Sage Court, Norman, OK 73072-3954, USA

Received: 3 July 2020 / Accepted: 23 October 2020

Abstract. This contribution deals with about selective conversion of heavy gas oils into middle distillates fuels that meet ultra-low sulfur and aromatic compound quality standards by using a novel NiWRu/TiO_2–γAl_2O_3 catalyst under typical hydrotreatment conditions. A diesel fuel fraction having sulfur, nitrogen and aromatics compound content of about 50 ppm, 10 ppm and 15 v%, respectively, was obtained when the reactor was operated at $T = 370$ °C, $P = 12.4$ MPa, LHSV = 0.5 h^{-1} and H_2/hydrocarbon ratio = 800 Nm^3/m^3. Titanium and ruthenium additives used in the preparation of the NiWRu/TiO_2–γAl_2O_3 catalyst, remarkably improved the catalytic activities for the hydrogenolysis, hydrogenation and hydrocracking reactions compared to the reference NiW/γAl_2O_3 catalyst. The coprecipitation of titanium and aluminum hydroxides produced a catalyst support having greater surface area, pore volume and surface acidity. An improvement in mechanical properties of the support extrudates was also observed. Characterization analysis by XPS, AUGER and XRD techniques of the TiO_2–γAl_2O_3 support suggested the formation of an aluminum-titanate mixed phase ($Al_xTi_yO_z$) having a non-well-defined stoichiometry. The NiW/TiO_2–γAl_2O_3 and NiWRu/TiO_2–γAl_2O_3 exhibited a greater surface dispersion of the supported nickel and tungsten species compared to the NiW/γAl_2O_3 catalyst. The promoter effect of ruthenium on the NiW bimetallic system caused a strong increase in both hydrogenolysis and hydrogenation reactions. Hydrodenitrogenation and hydrocracking reactions were also favored by the increase in the hydrogenation capacity and in the surface acidity of the catalyst. The highest conversion levels for all investigated reactions were obtained when the NiWRu/TiO_2–γAl_2O_3 catalyst was prepared by co-impregnation of Ni and Ru in a second step. This catalyst showed sulfur tolerance properties when the reaction was conducted in the presence of different H_2S partial pressures. The catalytic behavior of the NiWRu/TiO_2–γAl_2O_3 catalyst was explained by the existence of a promoting effect between separated Ni and Ru sulfides species and the NiWS phase (dual mechanism).

1 Introduction

The continued depletion of light crude reserves has made oil refineries to process larger amounts of heavy crudes. The processing of these heavy feedstocks differ markedly from light loads due to the presence of high molecular weight asphaltene molecules, high contents of sulfur, nitrogen and organometallic compounds, mainly V, Ni and Fe. Very few refineries in the world are configured to process heavy crudes. This is the reason behind large oil corporations for making significant capital investments to develop new catalytic processes and modernize their process units.

The oil refining industry has been forced to produce cleaner fuels and operate their units more efficiently to meet with strict environmental restrictions imposed by government agencies, and to convert more heavy feedstocks to satisfy fuels demand in the regional markets and to improve their profit margins. The Environmental Protection Agency (EPA) developed heavy duty highway diesel fuel standards which came into force from 2008, which required a 90% emission reduction from 500 ppm S heavy duty vehicle standards [1–3].

To fulfill these requirements, oil companies have been making important capital investment for modernizing their refineries through the acquisition of new technologies, supporting research projects for the development of new catalytic materials and optimizing their operations for producing gasolines and diesel fuels having very low level of sulfur and aromatic compounds. A maximum of 50 ppm S and 20 v% aromatic compounds in fuels is currently permitted in most of mature markets and countries in way of development [1–3]. The National

* Corresponding author: rprada@chasmtek.com

This is an Open Access article distributed under the terms of the Creative Commons Attribution License (https://creativecommons.org/licenses/by/4.0), which permits unrestricted use, distribution, and reproduction in any medium, provided the original work is properly cited.

Environment Agency (NEA) defined Ultra-Low Sulfur Diesel (ULSD) as diesel fuels with $\leq$ 50 ppm S. However, in some states in the US and countries in the European Union (EU), Japan, South Korea and South Africa, a maximum limit of 10 ppm S were established. Since 2003, a "zero" S with very low aromatic content (less than 1% by volume) in diesel fuels has been made available in Sweden. The new environmental regulations in the US and EU countries also require a significant reduction in the aromatic content in fuels. These regulations establish a maximum aromatic level in diesel of about 15 v%, and the content of polycyclic aromatic compound $<$ 2 v% [1, 4, 5].

Catalyst manufacturing companies have been responding to the needs of their customers by using new materials to develop a new generation of highly active and selective catalysts. These new catalysts must consume equal or less hydrogen than current catalysts and more resistant to the deactivation by coke and/or metal deposits. In these developments, the textural properties of the catalyst support must be adapted to the nature of the feedstock to be hydrotreated. New active metal formulations must be resistant to deactivation by poisoning under high H_2S and NH_3 partial pressures and the irreversible adsorption of highly condensed aromatic compounds. Furthermore, these metals must remain stable when the reactor operates under severe temperature and pressure conditions.

Significant technological progresses have been made in the last two decades to improve the performance of Hydrotreating (HDT) catalysts. New catalyst textures, with large pores, bimodal porosity, continue to be developed with some success. Binary metal oxides, such as TiO_2–γAl_2O_3, SiO_2–γAl_2O_3, ZrO_2–γAl_2O_3, TiO_2–SiO_2 found to be of increasing interest as Hydrodesulfurization (HDS) catalyst support due to high activity and selectivity, thus drastically decreasing the hydrogen consumption [1, 2, 6–13].

Additives based on titanium, magnesium, cerium and zirconium have given some promising results. These additives have shown to modify the surface properties of the support, the dispersion of the active phase and the interaction forces between the active phase and the substrate [2, 6, 14, 15]. Catalysts based on TiO_2 and TiO_2–γAl_2O_3 showed a remarkable increase in the catalytic activities for the aromatic Hydrogenation (HDA), Denitrogenation (HDN) and Hydrocracking (HCK) reactions and a significant improvement in the metallic dispersion and the surface acidity properties [9, 10, 12, 16–18].

The catalysts based on CoMo/γAl_2O_3 and NiMo/γAl_2O_3 are mainly used in the HDT processes due to their high efficiency in HDS and HDN. However, NiW/γAl_2O_3 based catalysts, which have a higher price, are employed in the production of low sulfur diesel, aromatics hydrogenation and hydrocracking due to their high capacity in hydrogenation. Whereas, its performance is still insufficient to reach the ULSD level required in the fuel markets [14, 15, 19]. The use of noble metals in combination with NiW, NiMo and CoMo bimetallic systems provide a greater capacity in hydrogenation and hydrogenolysis which offers alternatives for the development of new catalysts for the production of ULSD and low aromatics content [20–22]. Harris and Chianelli [23, 24] have observed that for the HDS reaction of DBT, catalyst based on RuS_2 was found to be the most active of the transition metal sulfides. Vrinat *et al.* [25], observed that the $Ni_xRu_{1-x}S_2$ mixed phase show remarkable HDS and HYD activity properties, higher than the activities observed for RuS_2, MoS_2, CoMoS and NiMoS phases. These results look promising for the development of new catalytic systems with improved activity for the desulfurization and deep hydrogenation of aromatic compounds from heavy gas oils.

In the above context, we have been working on developing a catalytic process for the selective conversion of heavy gas oils into middle distillates containing low level of sulfur, nitrogen and aromatic compounds. This hydrotreating and Mild Hydrocracking (MHCK) process, shown in Figure 1, combines different catalyst systems based on CoMoP/γAl_2O_3, NiMoP/γAl_2O_3 and NiWRu/TiO_2–γAl_2O_3. The CoMoP/γAl_2O_3 and NiMoP/γAl_2O_3 catalysts were developed for the HDS-MHCK and HDN-MHCK reactions, respectively [17, 26]. Whereas, the NiWRu/TiO_2–γAl_2O_3 catalyst was formulated for the desulfurization of dibenzothiophenes and its derivatives, the saturation of aromatics compounds and for the selective production of medium distillates. In this work, we show the results obtained during the development of the novel NiWRu/TiO_2–γAl_2O_3 based catalyst.

For this purpose, a series of catalysts based on NiW/γAl_2O_3, NiW/TiO_2–γAl_2O_3 and NiWRu/TiO_2–γAl_2O_3, having similar Ni and W composition, were prepared by co-precipitation of titania.

This method is widely used for the manufacture of industrial catalyst supports due to viability of subsequent commercial scaling. Also, proper selection of equipment and rigorous control on various parameters is crucial during the manufacturing process of catalyst support. The key parameters that play an important role in the manufacture of industrial catalyst supports are as follows: (i) the nature of the metallic salts, (ii) concentration of solids in solution, (iii) order and rate of addition of the acid-base solutions, (iv) co-precipitation temperature and pH, (v) aging time, (vi) gel filtration and washing conditions (pH and temperature), (vii) drying temperature, (viii) type of formulation operations (extrusion, spherization, granulation, tablets, etc.), (ix) calcination temperature and time.

The prepared catalysts were characterized by BET surface area, pore volume, surface acidity measurements using pyridine chemisorption, X-ray Photoelectron Spectroscopy (XPS) and Auger spectroscopy. Catalytic activity properties for the HDS, HDN, HDA and MHCK reactions were evaluated in a fixed bed pilot reactor, at 5.5 and 12.4 MPa total pressure and at 370 and 380 °C. Heavy gas oils feedstocks were previously hydrotreated using the CoMoP/γAl_2O_3 and NiMoP/γAl_2O_3 catalyst systems under typical MHCK conditions [26]. The role of titanium and ruthenium for improving the hydrogenolysis, hydrogenation and hydrocracking reactions were investigated.

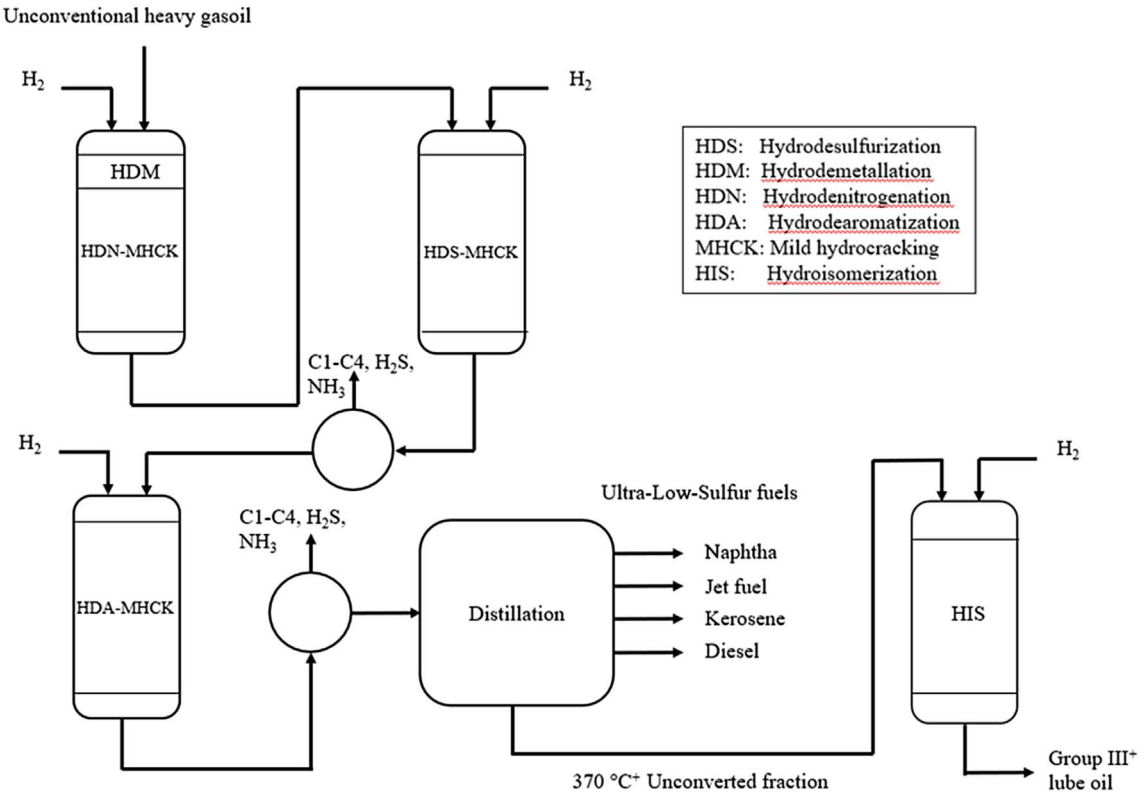

Fig. 1. Simplified scheme of the process for producing ultra-low-sulfur and aromatic middle distillate fuels from unconventional heavy gas oils.

2 Experimental methods

2.1 Catalyst preparation

The TiO_2–γAl_2O_3 catalyst support was prepared by the co-precipitation method from aqueous solutions containing $TiOSO_4$, $NaAl_2O_4$ and $Al_2(SO_4)_3$ salts. The obtained paste was filtered and then washed several times with hot deionized water until the level of SO_4^{-2} and Na^+ ions in the solid was less than 0.5 wt%. Subsequently, the solid was dried using the spray drying technique and then extruded into cylindrical particles having a diameter of 1.4 mm and a length of about 8 mm. The extrudates were dried and calcined at 500 °C for 4 h. The TiO_2 composition in the calcined material was 15 wt%. An alumina support was prepared from aqueous solutions containing $NaAl_2O_4$ and $Al_2(SO_4)_3$ salts following the same procedure described above.

Supported NiW-based catalysts were prepared by the pore-filling method (also known as incipient wetness impregnation) from aqueous solutions containing Ni and W metal salts. The pore-filling method commonly practiced in the catalyst industry has several advantages over other catalyst preparation methods such as: simple execution, good control of the active metals composition in the finished product, safer operation and low cost. The active metals were deposited on the γAl_2O_3 or TiO_2–γAl_2O_3 supports surface through two consecutive impregnation steps. In the first step, an aqueous solution of Ammonium Meta-Tungstate (AMW) was sprayed over 5 kg of the support extrudates in a rotary drum equipment and then the impregnated solid was aged for 2 h at room temperature under controlled moisture. Subsequently, the impregnated particles were dried in air flow at 120 °C for 2 h. In the second step, an aqueous solution containing nickel nitrate was sprayed over the solid. The aging and drying of the impregnated particles were carried out under the same conditions previously described. The dried solid was subsequently calcined at 550 °C for 4 h. Both NiW/TiO_2–γAl_2O_3 and NiW/γAl_2O_3 catalysts were prepared and used as reference materials.

Two NiWRu /TiO_2–γAl_2O_3 catalysts were prepared by co-impregnation of Ni and Ru and by doping the NiW/TiO_2–γAl_2O_3 catalyst with a Ru chloride solution. The latter catalyst is denoted in the following as NiW + Ru/TiO_2–γAl_2O_3. The aging and drying steps were carried out under the same conditions as described above. The chemical composition of the prepared catalyst was found to be 20 wt% WO_3, 6 wt% NiO and 0.6 wt% Ru, when analyzed by atomic absorption technique.

2.2 Adsorption properties of the metal ions solutions

To investigate the changes in pH due to the adsorption of metal ions on the γAl_2O_3 and TiO_2–γAl_2O_3 supports surface during the aging time, the following experiment was conducted. A 1.2M solution of Ammonium Meta-Tungstate solution was prepared and a 120 mL aliquot of this solution was taken and then contacted with variable quantities of

alumina support (from 5 to 80 g). The pH of the solution was determined every 2 h, which corresponds to the aging time employed for the catalyst preparations. The $W/\gamma Al_2O_3$ was dried at 60 °C for 4 h and then at 150 °C overnight. The same experiment was carried out but, in this case, a 0.55 M solution of nickel nitrate was used.

2.3 Characterization analysis

BET surface area and pore volume were performed using the multipoint method by N_2 adsorption on a Micromeritics ASAP 2400 instrument. Samples were first outgassed at 400 °C for about 4 h under vacuum before the analysis. Pore size distribution of the γAl_2O_3 and TiO_2–γAl_2O_3 catalyst and their corresponding NiW supported catalysts were determined from the N_2 desorption isotherm.

X-ray diffraction patterns of the catalyst supports were performed with a Phillips 1730/10 powder diffractometer using nickel filtered Cu K_α radiation ($\lambda = 1.5418$ Å).

Total surface acidity has been determined gravimetrically using pyridine as a probe molecule adsorbed on the surface. The total irreversible adsorbed pyridine amounts were measured at 100 °C. Result was expressed as millimole of adsorbed pyridine per gram of support.

Zero Point of Charge (ZPC) of the solids was determined using the mass titration technique. Different amounts of solid were added to a fixed volume of 0.1 M NaCl solution contained in plastic bottles and then sealed, thus obtaining samples containing solid fractions ranging from 0.1 to 5 wt%/v%. The samples were left equilibrating for 24 h and pH of the supernatant liquid was measured. The ZPC was determined from the asymptotic value of equilibrium pH *vs.* solid fraction curves.

Bulk crushing strength was determined by using the Shell N^o SMS1471 method described as follows. The samples were first dried in an oven at 300 °C during 2 h. About 20 cc of the sample was taken and placed in the cell and covered with 5 cc of steel balls diameter 3 mm, and then put on the anvil of the stress transducer. Increasing force is applied by the piston to the catalyst in stages of 3 min. The fines obtained at the different pressure stages are separated by sieving, and weighed: particles which pass through the mesh of a sieve of opening 420 µm are considered as fines. The Bulk Crushing Strength is estimated according to the following equation:

$$P = \frac{F}{A},$$

where F is the force to be applied on the catalyst in kgf to produce 0.5% fines and A is the cross-sectional area of the sample holder in cm^2.

X-ray Photoelectron Spectra (XPS) and Auger Electron Spectra (AES) of the catalysts were recorded using a Leybold Heraeus LHS-121 apparatus equipped with a computer system, which allows the determination of peak areas. Analyzes were performed in an ultra-high vacuum system at a base pressure of 1.2×10^{-9} mbar using an AlK_α radiation ($E = 1486$ eV) as the source. All samples were ground and then pressed into the sample holders before the analysis. Signals corresponding to C_{1s}, O_{1s}, Al_{2p}, Ti_{2p}, Ni_{2p}, W_{4f} and Ru_{3d} energy levels were recorded. The C_{1s} energy level (284.5 eV) was taken as a reference. Atomic surface concentration of supported elements (e) was evaluated from the peak integrated areas and the sensitivity factors provided by the equipment manufacturer.

2.4 Catalytic activity

Sulfur content in both VGO feedstock and reaction products was determined by X-ray fluorescence technique (ASTM D4294) using Philips PW2400 Sequential Wavelength Dispersive X-Ray Fluorescence Spectrometer while the nitrogen content was determined by Chemiluminescence method (ASTM D4629) on a Dohrmann Total Nitrogen Analyzer Type DN-10. Mass Spectrometry coupled with a Gas Chromatography (GC-MS) was used to measure the aromatic (ASTM- D3239) and saturated fractions (ASTM D2786). These fractions were separated by High Pressure Liquid Chromatography (HPLC) technique prior the analysis. The middle distillate and unconverted fractions were determined by Simulated Distillation (SimDis) technique (ASTM D2425) using a Kratos MS-25Q equipment.

Activity properties for the HDS, HDN, HDA and MHCK reactions were evaluated in a high-pressure fixed bed pilot reactor. About 60 cc of catalyst were pre-sulfided using 2 wt% CS_2 in a light gasoil and hydrogen flow. The activation was carried in two successive steps; at $T = 260$ °C for 5 h and at $T = 350$ °C for 8 h, $P = 2.8$ MPa, LHSV = 1.5 h^{-1} and H_2/hydrocarbon ratio = 400 v/v.

The catalytic properties of the different prepared catalysts were determined using a vacuum gas oil containing the following properties: S = 0.394 wt%, N = 460 ppm, aromatic: 55 v% and 370 °C$^+$ fraction = 42 V%. The activity tests were carried out at $T = 380$ °C, $P = 5.5$ MPa, H_2/hydrocarbon = 1000 v/v, LHSV = 0.55 h^{-1} and 50 h reaction time.

3 Results

Table 5 shows the results of the textural, surface charge properties corresponding to the TiO_2–γAl_2O_3, γAl_2O_3, anatase (TiO_2) catalyst supports and textural, mechanical properties and chemical composition results of the $NiWRu/TiO_2$–γAl_2O_3, NiW/TiO_2–γAl_2O_3 and $NiW/\gamma Al_2O_3$ catalysts. Noticeable differences were observed between the analyzed supports. When the support was prepared by co-precipitation of Ti and Al hydroxides, significant in surface area and pore volume was observed. The mean pore diameter significantly decreased. The ZPC value observed for the TiO_2–γAl_2O_3 support is intermediate between the γAl_2O_3 and anatase.

All catalyst supports experienced a decrease in BET surface area and pore volume after the metal deposition. As expected, the $NiW/\gamma Al_2O_3$ catalyst showed the lower surface area and pore volume values. The addition of low levels of ruthenium during the preparation of the $NiWRu/TiO_2$–γAl_2O_3 catalyst did not affect their physical

Table 1. Textural, ZPC, crushing strength and chemical composition properties of supports and NiW and Ru catalysts.

Sample	BET Surface area (m^2/g)	Pore volume (cc/g)	ZPC (pH unit)	Crushing strength (Kgf/cm^2)	Chemical composition (wt%) $NiO/WO_3/RuO_2$
15 wt% TiO_2–γAl_2O_3	330	0.93	7.1	–	–
γAl_2O_3	264	0.65	8.0	–	–
TiO_2	58	0.19	6.8	–	–
$NiW/\gamma Al_2O_3$	170	0.45	–	6.8	6.2/20.1 /–
NiW/TiO_2–γAl_2O_3	220	0.52	–	9.4	6.0/19.9/–
$NiWRu/TiO_2$–γAl_2O_3	230	0.55	–	9.4	6.1/20.0/0.6

and chemical properties. The NiW/TiO_2–γAl_2O_3 catalyst showed improved mechanical properties compared to $NiW/\gamma Al_2O_3$ catalyst. Results of Table 1 also indicated that all prepared catalysts show similar W and Ni composition.

Table 2 shows the pore diameter distribution, obtained from the nitrogen adsorption-desorption isotherms, for the TiO_2–γAl_2O_3 and γAl_2O_3 catalyst supports. A narrow pore diameter distribution was observed for the TiO_2–γAl_2O_3 support. Most of the pores had a diameter less than 90 Å. In contrast, the alumina support showed a wide distribution of pore diameter, most of them had a diameter between 90 Å and 300 Å.

The surface acidity properties of the γAl_2O_3, TiO_2–γAl_2O_3 supports and the NiW/TiO_2–γAl_2O_3 catalyst were determined using the pyridine chemisorption technique in the temperature range between 100 and 400 °C. According to literature weak acid sites are classified as weak, moderate and strong acid sites, are determined by the amount of pyridine irreversibly adsorbed at ≤250 °C, 250–350 °C and $T > 350$ °C, respectively [27]. The results shown in Figure 2 clearly indicate a strong increase in the number and strength of the acid sites for the NiW/TiO_2–γAl_2O_3 catalyst and the TiO_2–γAl_2O_3 support with respect to the γAl_2O_3.

Figure 3 shows the results of the X-ray diffraction analysis corresponding to the TiO_2, γAl_2O_3 and TiO_2–γAl_2O_3 catalyst supports. A wide diffraction pattern is observed for the TiO_2–γAl_2O_3 support for values of 2θ between 20° and 50°. There is no clear evidence on the formation of anatase for 15 wt% TiO_2 composition in γAl_2O_3.

The results of the XPS and AES analyzes corresponding to the TiO_2, γAl_2O_3 and TiO_2–γAl_2O_3 catalyst supports are shown in Table 3. The XPS binding energies corresponding to the Al_{2p}, $Ti_{2p3/2}$ and O_{1s} levels and the Auger electronic transitions $Ti_{(LMM)}$ and $O_{(KLL)}$ are reported. For the TiO_2–γAl_2O_3 support, no significant differences were observed between the binding energies of the Al_{2p} and $Ti_{2p3/2}$ levels with respect to the position of the signals observed for the TiO_2 and γAl_2O_3. However, it was observed that the width of the $Ti_{2p3/2}$ signal was 2.4 eV for the TiO_2 and 3.4 eV for the TiO_2–γAl_2O_3 support. The binding energy value of the O_{1s} level observed for the TiO_2–γAl_2O_3 support was 0.7 eV lower with respect to alumina and 1.1 eV higher with respect to TiO_2. The Auger analyzes show more significant differences with respect to the results obtained by XPS analyzes. For the TiO_2–γAl_2O_3 support, there is a difference of about 1.3 eV lower with respect to anatase for the energy level $Ti_{(LMM)}$ whereas, an increase of approximately 1.2 eV was observed with respect to the γAl_2O_3 and a decrease of about 3.2 eV with respect to TiO_2 for level energy $O_{(KLL)}$.

The XPS characterization technique provides information regarding the nature and surface dispersion of the supported metal oxide precursor phases. Table 4 shows that the percentage metal surface dispersion, given by the relative W and Ni intensities ($Ie/\Sigma Ie$; where e = element) are practically the same for both $NiWRu/TiO_2$–γAl_2O_3 and NiW/TiO_2–γAl_2O_3 catalysts. However, for the $NiW/\gamma Al_2O_3$ catalyst the surface metal dispersion values are significantly lower.

Table 2. Pore size distribution of γAl_2O_3 and TiO_2–γAl_2O_3 catalyst supports.

Pores diameter (Å)	γAl_2O_3	TiO_2–γAl_2O_3
<30	2	5
30 to <90	38	56
90 to <150	34	25
150 to <300	19	6
>300	7	8

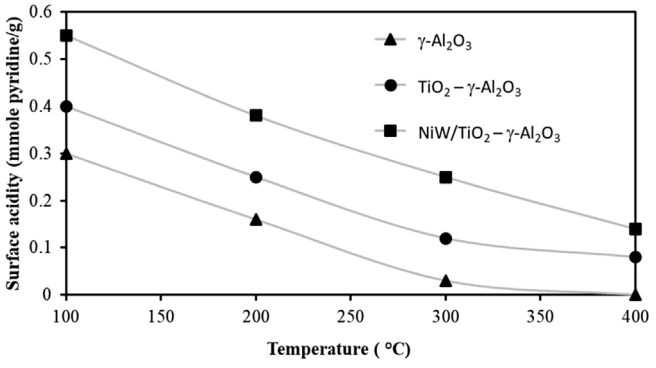

Fig. 2. Acid strength distribution corresponding to the catalyst supports.

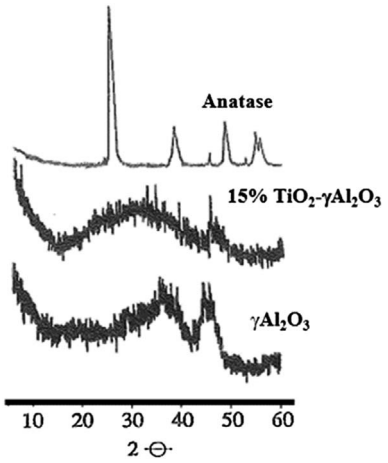

Fig. 3. XRD patterns corresponding to γAl_2O_3 and TiO_2–γAl_2O_3 catalyst supports.

Table 3. Binding energies corresponding to different supports.

	Al_{2p}	$Ti_{2p3/2}$	O_{1s}	$Ti_{(LMM)}$	$O_{(KLL)}$
TiO_2–γAl_2O_3	74.2	458.6	530.6	380.0	508.8
γAl_2O_3	74.0	–	531.3	–	507.6
TiO_2	–	458.7	529.5	381.3	512.0

Table 4. Metal surface dispersion of the different NiW supported catalysts.

	$IW_{4f}/\Sigma Ie$ (%)	$INi_{2p}/\Sigma Ie$ (%)	$Ru_{3d}/\Sigma Ie$ (%)
$NiWRu/TiO_2$–γAl_2O_3	8.0	4.5	1.0
NiW/TiO_2–γAl_2O_3	7.9	4.4	–
$NiW/\gamma Al_2O_3$	5.5	3.9	–

$\Sigma Ie = I\ W_{4f} + INi_{2p} + I\ Ru_{3d} + IAl_{2s} + I\ Ti_{2p}$.

The conversion in HDS, HDN, HDA and MHCK corresponding to $NiW/\gamma Al_2O_3$ and $NiW/\gamma TiO_2$–Al_2O_3 catalysts are shown in Figures 4a and 4b, respectively. The addition of 15 wt% TiO_2 in the alumina preparation not only produced a significant improvement in the activity for hydrogenolysis and hydrogenation reactions, but also showed a moderate conversion of the heavy fraction (370 °C$^+$) into middle distillates cut. As it can be seen, the level of conversion for all investigated reactions significantly increases when Ru in employed as an additive in the $NiW/\gamma TiO_2$–Al_2O_3 catalyst formulation. These conversions were defined by determining the percentage difference in the level of S, N and aromatics from feedstock to the final product. The MHCK conversion was estimated by determine the percentage difference of the 370 °C$^+$ distillation fraction from feedstock to the final product. The largest increases in conversion levels were observed for HDA and HDS reactions. The catalyst prepared by co-impregnation of Ni and Ru resulted the most active.

Table 5. Properties of the diesel fraction.

	$NiWRu/TiO_2$–γAl_2O_3	NiW/TiO_2–γAl_2O_3
S (ppm)	50	300
N (ppm)	10	100
Aromatics	15	25
Cetane index	54	40
Cloud point (°C)	25	0

4 Discussion

The above results clearly showed how the textural and mechanical properties, the acidity strength and distribution, the surface-active metal dispersion and catalytic activity properties can be strongly influenced by the use of titanium additive in the alumina preparation and ruthenium in combination with nickel and tungsten active metals supported. To facilitate the interpretation of our results, let's us divide the discussion in five sections.

- Section 4.1: We will discuss the role of titanium on the texture, structure of the metal oxides phases, surface charge and acidity properties of TiO_2–γAl_2O_3 catalyst support.
- Section 4.2: We will discuss the results of the physicochemical characterization of the $NiW/\gamma Al_2O_3$ and NiW/TiO_2–γAl_2O_3 catalysts.
- Section 4.3: We will try to correlate the results of the characterization analysis with the catalytic activity of the $NiW/\gamma Al_2O_3$ and NiW/TiO_2–γAl_2O_3 catalysts.
- Section 4.4: We will investigate the role of ruthenium on promoting the hydrogenolysis and hydrogenation reactions. We will also try to correlate the activity results of the different prepared catalysts on the basis of two theoretical models proposed in the literature to explain the origin of the catalytic synergy in HDS and HYD reactions between the elements of groups VI and group VIII of the periodic table.
- Section 4.5: We will show the activity results obtained with the $NiWRu/TiO_2$–γAl_2O_3 catalyst for the production of ULSD.

4.1 Role of titanium on the textural, structure of the metal oxides phases, surface charge and acidity properties of TiO_2–γAl_2O_3 catalyst support

Different additives have been employed to improve the activity and selectivity properties of HDT and HCK catalysts for following reasons: i) to improve the dispersion of the active phases, ii) to increase the surface acidity of the support to selective convert heavy paraffins into lighter

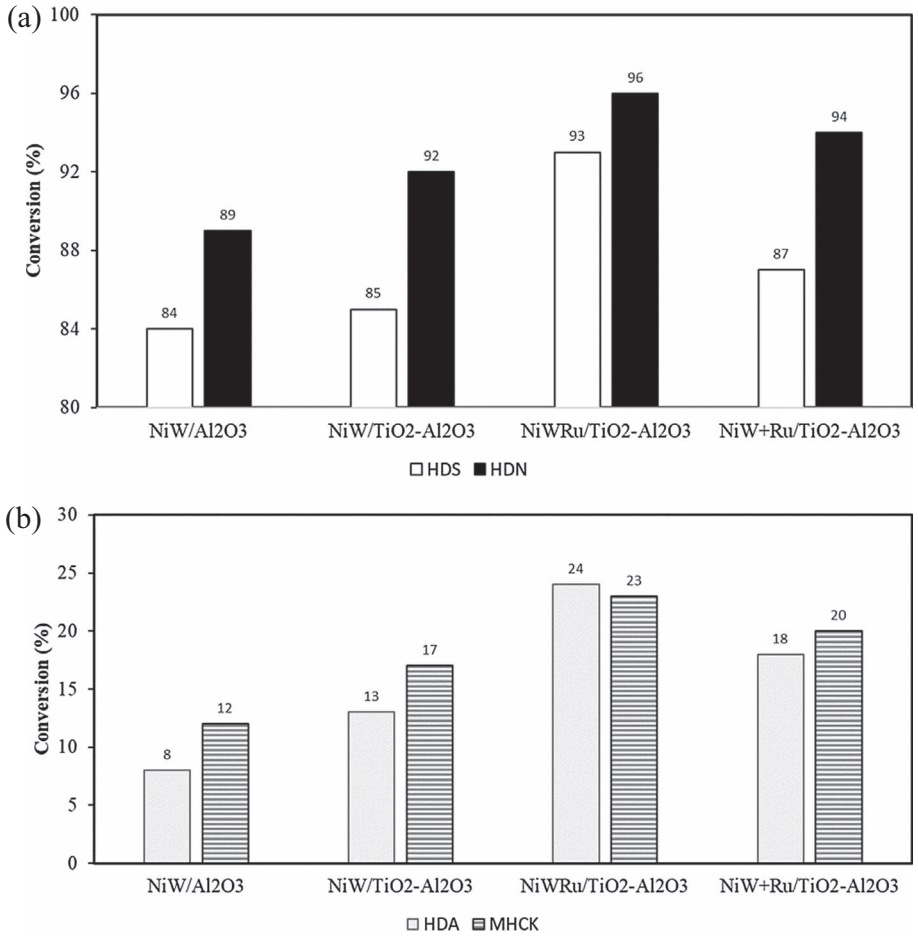

Fig. 4. (a) Conversion in HDS and HDN for the different prepared catalysts at $T = 380$ °C, $P = 5.5$ MPa, H_2/hydrocarbon = 1000 v/v, and LHSV = 0.55 h^{-1}. (b) Conversion in HDA and MHCK for the different prepared catalysts at $T = 380$ °C, $P = 5.5$ MPa, H_2/hydrocarbon = 1000 v/v, and LHSV = 0.55 h^{-1}.

products, iii) to increase the mechanical properties of the alumina support, iv) to avoid the formation of $Co(Ni)Al_2O_4$ phase, thereby increasing the actives Co(Ni) surface species and v) to reduce the deactivation of the catalyst *via* coke formation and deposition inside the pores [9, 16, 17, 26].

Phosphorous, silica, boron and fluorine additives have been widely used to improve the acidity properties of γAl_2O_3 support in conventional hydrocracking catalysts. However, these additives have shown some limitations to increase the hydrogenation capacity of aromatic compounds. Later, additives based on titanium, magnesium, cerium and zirconium were used, which have given some promising results. These additives have been shown to modify the surface properties of the support, the dispersion of the active phase and the interaction force between the active phase and the substrate [2, 6, 9, 16]. Catalysts based on TiO_2 showed a remarkable increase in the catalytic activities for the HDA, HDN and HCK reactions and a significant improve in the metallic dispersion and the surface acidity properties [9, 10, 12, 16–18]. Given the benefits provided by TiO_2 on the improvement of the activity properties for the above-mentioned reactions, we have decided to develop a new catalyst for producing ULSD from VGO and non-conventional heavy fractions. The use of TiO_2–γAl_2O_3 support in combination with NiWRu active metals provide additional performance benefits for the aforementioned reactions than the conventional CoMo and NiMo bimetallic systems.

During the co-precipitation step of the titanium and aluminum hydroxides, significant changes in the rheological properties of the material were observed. As the titanium content in the solid increased, it was observed that the precipitated acquired a plastic consistency that made it difficult to remove undesirable ions (Na^+ and $SO_4^=$) during the filtration and washing steps. For the support containing 20 wt% TiO_2, it was a major challenge to efficiently remove these impurities at levels below 0.5 wt%, since at higher levels, these impurities can affect the textural properties, surface acidity by creating strong Bronsted acid sites, lower ZPC which affect the adsorption capacity of metal ions and the mechanical strength properties of the support. The supports prepared with TiO_2 contents between 10 wt% and 15 wt% showed the best rheological properties for filtration, washing, drying and extrusion operations, so much so that a low concentration of binder was required, in comparison with aluminum hydroxide xerogel, to achieve

an efficient peptization of the material. In view of the rheological properties of the material and its peptizing properties, the extrusion operation turned out to be easy. This behavior could be related to the increase in the mechanical properties observed for the TiO_2–γAl_2O_3 support with respect to the γAl_2O_3. An optimum BET surface area and pore volume value were achieved for 15 wt% TiO_2 composition in γAl_2O_3. This same behavior was observed in different published studies when the TiO_2–γAl_2O_3 support was prepared using precipitation methods [8, 12, 28, 29]. Based on these results, we decided to use the 15 wt% TiO_2–γAl_2O_3 support for the development of the improved HDS-HDA catalyst.

From Table 2, a high proportion of mesopores having a diameter lower than 90 Å was observed for the 15 wt% TiO_2–γAl_2O_3 support. In contrast, the alumina support showed a wide pore sizes distribution, most of them had a diameter greater than 90 Å. The differences in pore diameter distribution have important implications related to the amount of active metals that can be deposited in the different pores. It also seems likely that a large proportion of acid sites are located in small pores. The cracking of long paraffins, hydrogenolysis of carbon-metal bond, and hydrogenation reactions of large molecules could preferentially take place in the large pores or outside them. The porosity of the support plays an important role in the activity and selectivity of the catalyst as well as, in the control of the deactivation by deposits of coke or formation of nickel, vanadium and other metal sulfides present in the feedstock. This is the reason why there is a large variety of industrial HDT and HCK catalysts which are recommended by their manufacturers according to the composition of the oil fraction to be hydroprocessed.

The ZPC value decreased progressively when the TiO_2 content in the TiO_2–γAl_2O_3 catalyst support was increased. Results from Table 1 showed that for the 15% TiO_2–γAl_2O_3 support, the ZPC value is intermediate between those ones observed for γAl_2O_3 and TiO_2. This trend agrees with those observed by several investigators that reported for TiO_2–γAl_2O_3, γAl_2O_3 and TiO_2 supports, ZPC and IEP values about 6.0, 8.0 and 5.8 pH units, respectively [30]. Bonsack [31] reported for anatase, Isoelectric Point (IEP) values in the range of 5.8–6.5 pH unit whereas, Vasquez-Garrido *et al.* [11] and Guevara-Lara *et al.* [32] observed that for 95 wt% TiO_2 in alumina, the support exhibited a ZPC value of 4.9 pH unit. The observed differences between the ZPC values obtained in this work in comparison with those reported in the literature for TiO_2–γAl_2O_3 and TiO_2 supports can be explained by the use of different titration methods (KOH *vs.* NaCl), differences in TiO_2 composition in the mixed oxide support and the presence of impurities in the samples.

The number and strength of acid sites increased progressively when the TiO_2 content in the TiO_2–γAl_2O_3 catalyst support was increased. Our results suggest the existence of a parallel trend between the increase in BET surface area, pore volume and the surface acidity. As mentioned above, a large proportion of acidic sites are located in small pores. This same parallelism can be observed in other works published in the literature where support was prepared by the coprecipitation method and for TiO_2 composition $\leq$ 20 wt% [12, 28, 29]. Other methods of TiO_2–γAl_2O_3 support preparation (sol-gel, impregnation, grafting) showed different behavior [29]. When the binary TiO_2–γAl_2O_3 oxide was prepared by impregnation of titanium isopropoxide or by reaction between the hydroxyl groups of γAl_2O_3 powder with $TiCl_4$ vapors, the BET surface gradually decreased with increasing of TiO_2 content. Analysis conducted by Temperature Programmed Desorption (TPD) of ammonia showed that the maximum desorption temperature did not change with the TiO_2 content for the impregnated samples but its intensity became lower and shifted to high temperatures with the increasing of grafting time. These results suggest differences in structure and composition of the titanium and aluminum phases when TiO_2–γAl_2O_3 supports are prepared by different methods.

The XRD, XPS and AES characterization techniques enable to identify the different titanium and aluminum phases present in catalysts supports. The X-ray diffraction analyzes were not sensitive enough to clearly detect the formation of titanium oxide phases in the TiO_2–γAl_2O_3. It was only at high titanium loading that discrete TiO_2 crystallites were detected [31]. The broad and not well-defined diffraction pattern observed for the TiO_2–γAl_2O_3 support is characteristic of solids having a completely amorphous structure [12]. However, the XPS and AES analyzes showed significant differences in the binding energies corresponding to $Ti_{2p3/2}$, $O_{1S,}$ energy levels and $Ti_{(LMM)}$, $O_{(KLL)}$ electronic transitions which suggests that the titanium and aluminum atoms could be found in a different chemical environment than in anatase and alumina. Based on these observations, an aluminum titanate-like phase ($Al_xTi_yO_z$) containing a non-well-defined stoichiometry could be present in the TiO_2–γAl_2O_3 support. This phase could be formed from the titanium and aluminum coprecipitated hydroxides during the calcination step according to equation (1):

$$TiAl_4(OH)_{16} \rightarrow TiAl_2O_5 + \gamma Al_2O_3 + 8H_2O \quad (1)$$

$TiAl_2O_5$ was obtained starting from a mechanical mixture of TiO_2 and αAl_2O_3 at very high temperature ($T > 1400$ °C) [33, 34]. Nanocrystals of $TiAl_2O_5$ were also observed to be formed from a $Ti_{0.2}Al_{0.8}O_x$ film annealed at 900 °C, according to equation (2) [35]:

$$(TiO_2)_{1/3}(Al_2O_3)_{2/3} \rightarrow 1/3\,TiAl_2O_5 + 1/3\,\alpha Al_2O_3. \quad (2)$$

Characterization analysis by diffuse reflectance spectroscopy (DRS) of a series TiO_2–γAl_2O_3 supports that were prepared by co-precipitation of aluminum and titanium isopropoxides indicated that for low $TiO_2/TiO_2 + Al_2O_3$ molar ratio, titanium would be linked to aluminum, through oxygen bridges (Ti–O–Al) and as the titanium loading increases a high proportion of Ti–O–Ti linkages are present. Titanium in anatase is in octahedral coordination whereas, aluminum atoms in the alumina are located in both tetrahedral and octahedral coordination. At low titanium loadings, part of the titanium atoms can replace the aluminum atoms in tetrahedral geometry surrounded by four oxygen atoms. During the formation of aluminum

titanate, a random distribution of titanium in octahedral and tetrahedral coordination are present [29]. As the size of the Ti atoms are greater than the Al atoms, their insertion into the alumina crystalline lattice can create distortions of both tetrahedral and octahedral sites modifying their textural, surface charge and acidity properties. The $TiO_2/TiO_2 + Al_2O_3$ molar ratio of 0.5 corresponds to the theoretical formulation of aluminum titanate. This ratio represents a limit to the amount of titanium entering the alumina network. Experimental and computational studies of γ-Al_2O_3 show that $30 \pm 2\%$ of Al ions occupy tetrahedral interstitial sites in the face centered cubic oxygen structure, and the rest octahedral sites [36]. According to this estimate, the Al_{th}/Al_{oh} atomic ratio in γ-Al_2O_3 is about 0.43. In this work, the $TiO_2/TiO_2 + Al_2O_3$ molar ratio composition is about 0.19 (Ti/Al = 0.46). Therefore, there are enough tetrahedral sites in the γ-Al_2O_3 to be occupied by the titanium atoms to form a mixed oxide compound having a not-well defined stoichiometry ($Al_xTi_yO_z$) and a very small fraction of titanium atoms will be as TiO_2.

An indirect experimental evidence that suggested the formation of an Al_xTi_yOz phase is given by DRS analysis of a series of $CoMo/TiO_2$–γAl_2O_3 catalysts [12]. Decrease in signals intensities corresponds to Co^{+2} in tetrahedral coordination ($CoAl_2O_4$-like phase) and increase of Co_3O_4 surface composition was observed when the titanium loading was progressively increased in the 0–0.5 $TiO_2/TiO_2 + Al_2O_3$ atomic range composition.

In summary, the benefits provided by titanium on the textural, structure of the metal oxides phases, surface charge and acidity properties of TiO_2–γAl_2O_3 depend on the following support preparation parameters:

- Synthesis method employed (co-precipitation [8, 10, 12, 15, 28, 30], sol-gel [14, 21, 37, 38], impregnation [30], grafting [18, 29], co-templates [39]).
- Titanium and aluminum precursors compounds employed in the co-precipitation (Ti and Al isopropoxides, $TiOCl_2$, $TiOSO_4$, etc.).
- Titanium composition in the TiO_2–γAl_2O_3 support.
- Above described experimental conditions.
- Type and level of impurities present in the solid.

This satisfactorily explains the existent controversy in the literature about the role of titanium as an additive to improve the physicochemical and surface properties of alumina.

4.2 Physico-chemical characterization of the NiW/γAl_2O_3 and NiW/TiO_2–γAl_2O_3 catalysts

Results of Table 1 indicated that both γAl_2O_3 and TiO_2–γAl_2O_3 supports underwent a significant decrease in surface area and pore volume as a consequence of the metal deposition in their pores. The NiW/ TiO_2–γAl_2O_3 catalyst showed higher BET surface area and pore volume values than the NiW/ Al_2O_3 catalyst. The number and strength of the acidic sites of the NiW/TiO_2–γAl_2O_3 catalyst increased significantly as compared to the surface acidity of the TiO_2–γAl_2O_3 support.

Let us first discuss the observed behavior during the preparation of the NiW/γAl_2O_3 and NiW/ TiO_2–γAl_2O_3 catalysts. Subsequently, we will try to interpret our results taking into account fundamental studies published in the literature dealing with the chemistry of Ni and W species in solution and their adsorption mechanism on γAl_2O_3 and TiO_2–γAl_2O_3. Finally, we will try to correlate the characterization results with the catalytic behavior of these catalysts.

Sequential impregnation steps are used in the practice to minimize the impact of the high density, viscosity, stability and contact angle properties of the metallic solution, drop pressure and capillary diffusion time. These effects were also observed in previous work [17, 26]. Sequential impregnations were carried out where the tungsten was deposited first on the alumina support and then the nickel. Steps of aging and drying were carried in between and calcination was made after the nickel deposition. During aging step, there is some diffusional migration of the metallic ions inside the pores. We have previously observed that aging time is a critical experimental parameter to control. Air bubbles inside the pores are shifted during the liquid capillary diffusion, the metallic ions start adsorbing and smaller crystallites of active metal precursors are deposited on the internal surface of the solid. The adsorption of the ionic species on the surface cause changes in the solution pH. The aging time controls the metallic surface dispersion and the elemental radial distribution profiles through the cross section of the support extrudates.

During the drying process, elimination of water from the pores and simultaneous crystallization of the precursor active phases takes place through supersaturation of the solution. Changes in the density and viscosity of the metal solution inside the pores affect the rate of drying. On supports with narrow pores size distribution, such as TiO_2–γAl_2O_3 support, the water is removed in concentric layers starting from the extrudate outer surface causing accumulation of precursor salts in the inner surface as the rate of evaporation is slow in relation to the rate of diffusion of the solute. In catalyst supports with a broad pore size distribution, such as γAl_2O_3, the pores having large diameter will empty themselves on their solution, and accumulation of precursor salts within the smaller pores take place. A fast drying provokes metal removal from the impregnated support by the steam generated. A slow drying produces homogeneous catalyst but can impact on the catalyst production cost. The aging and drying experimental conditions must be optimized according to the pore size distribution of the catalyst support. Both processes can have a strong influence on the BET surface area, pore volume and diameter distribution, metal dispersion, elemental radial distribution profile and chemical composition of the finished catalyst [17].

The results of the adsorption properties of the metallic solutions on both TiO_2–γAl_2O_3 and γAl_2O_3 supports are shown in Figure 5. The initial pH of the Ammonium Meta-Tungstate solution was 3.86 units. When 5 g of alumina were added to the solution, the pH increased sharply (to about 6.6 pH units) and then, it increased moderately increased with the amount of support added. A maximum

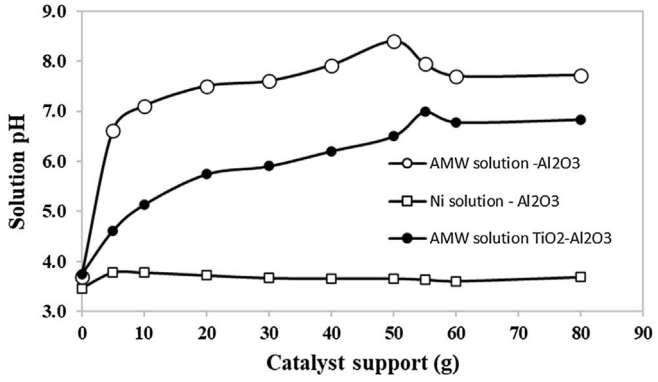

Fig. 5. Variation of the Ammonium Meta-Tungstate and nickel nitrate solution pH as a function of the amount of γAl_2O_3, TiO_2–γAl_2O_3 and $W/\gamma Al_2O_3$ added.

solution pH (8.4 units) was achieved after adding 50 g of alumina. However, when added 50 g of alumina into 120 ml of DI water a pH of about 7.4 units after 2 h contact time was observed. The pH decreased to 7.7 units when 60 g of support were added and then the pH remained constant after 80 g of alumina added. For the TiO_2–γAl_2O_3, it was observed that the solution had a pH = 6.8 units after adding 80 g of support into the AMW solution. Although the volume of the Ammonium Meta-Tungstate solution was about 2.2 and 1.6 times greater than the pore volume of the γAl_2O_3 and TiO_2–γAl_2O_3 for 80 g of support, respectively, however, it would be expected that similar changes in the solution pH may occur inside the pores when impregnation is carried out by the pores filling method.

In the case of the experiments conducted with the $W/\gamma Al_2O_3$ and nickel solution, no significant variation of the solution pH was observed as a function of the amount of catalyst support added.

Further we have evaluated the effect of pH on the chemical equilibrium of the tungsten ionic species in solution and their adsorption mechanism on alumina. Some relevant studies from the literature indicated that pH, metal concentration of the solution and ZPC of the support controls the amount and structure of the tungsten oxide species on the surface [40–43]. At solution pH higher than 7.8 and 1 M in tungsten, tetrahedral WO_4^{2-} species were observed. At pH values between 5.7 and 7.8, $W_{12}O_{42}^{12-}$ polyanion were formed while at lower pH, octahedral coordinated $W_{12}O_{39}^{6-}$ polyanions were observed. The following chemical equilibrium between tungsten ions was established as a function of the pH's of the exchanging solution.

$$W_{12}O_{39}{}^{6-}{}_{(oh)} \overset{pH\leq 5.7}{\Longleftrightarrow} W_{12}O_{42}{}^{12-}{}_{(oh)} \overset{pH\leq 7.8}{\Longleftrightarrow} 12\ WO_4{}^{2-}{}_{(th)}. \quad (3)$$

According to equation (3) and the results of Figure 5, the $W_{12}O_{39}^{6-}$ ionic species are present in the AMW impregnating solution. The abrupt change in pH observed after adding 5 g of the γAl_2O_3 support into the AMW solution is mainly due to the neutralization reaction between the basic OH groups of the support and the acidic OH groups of the tungsten ions during the adsorption process. The chemical equilibrium shifts towards to the right and $W_{12}O_{40}^{8-}$ ionic species are formed from pH > 5.7. Both tetrahedral WO_4^{2-} and octahedral $W_{12}O_{42}^{12-}$ anions co-exist at solution pH near to 7.8 units. After adding 60 g of γAl_2O_3 support to the tungsten solution, the pH dropped from 8.2 to about 7.8 units because the acid sites of the γAl_2O_3 support neutralize the hydroxyl ions in solution. For the TiO_2–γAl_2O_3 support, the $W_{12}O_{42}^{12-}$ ions are those that are adsorbed on the support surface during the aging time, thus the solution pH was 6.8 after adding 80 g of support.

The hydroxyl groups of both anatase and alumina surface in solution tend to be either positively or negatively charged below or above the ZPC of these compounds. Results of Table 5 indicated that the ZPC for γAl_2O_3 and anatase was 8.0 and 6.8 pH units, respectively. Based on the oxide charging mechanism proposed in the literature [28, 41], two chemical equilibria are established for TiO_2 as a function of the pH (Eq. (4)).

$$TiOH_2^+ \overset{H^+}{\Leftarrow} TiOH\,O \overset{H^-}{\Rightarrow} TiO^- + H_2O. \quad (4)$$

Above the ZPC of TiO_2, the hydroxyls groups of this compound tend to be negatively charged by formation of the deprotonated titania species (TiO^-) affecting the tungsten anions to be adsorbed on the titania surface due to the electrostatic repulsions with the negative charged surface. The alumina surface is charged positively below its ZPC; therefore, tungsten anions tend to be adsorbed due to electrostatic attraction with the surface.

After tungsten deposition on both γAl_2O_3 and TiO_2–γAl_2O_3 supports surface, we determined the ZPC before proceeding with the second impregnation step with nickel nitrate. ZPC values corresponding to $W/\gamma Al_2O_3$ and W/TiO_2–γAl_2O_3 samples decreased to about 5.4 and 5.9 pH units, respectively. The pH of the $Ni(NO_3)_2$ solution was about 3.7 units. At that solution pH, electrostatic repulsions between Ni^{2+} ions and the support surface are produced. During the drying step, crystallization and deposition of Ni salts take place on top of the tungsten adsorbed species as well as on the γTiO_2–Al_2O_3 uncovered surface is produced. When the solid is calcined, Ni^{2+}/WO_4^2, and separated NiO and WO_3 species were identified. The presence of TiO_2 in γAl_2O_3 mitigates the formation of $Ni_{(th)}$ ($NiAl_2O_4$ like-phase) while, the surface concentration of $Ni_{(oh)}$ oxide species increases [28].

4.3 Catalytic properties of the $NiW/\gamma Al_2O_3$ and NiW/TiO_2–γAl_2O_3 catalysts

As indicated in the results of the catalytic activity tests, the NiW/TiO_2–γAl_2O_3 catalyst was significantly more active for the hydrogenolysis, hydrogenation and hydrocracking reactions than the reference $NiW/\gamma Al_2O_3$ catalyst. On the other hand, the characterization studies indicated an improvement in the physico-chemical and surface properties when titanium is employed as an additive to alumina. These results would partially explain the catalytic behavior observed for the NiW/TiO_2–γAl_2O_3 catalyst. However, other important factors need to be considered to arrive for more complete interpretation, such as: i) differences on

the nature and composition of the nickel and tungsten supported phases, and ii) reducibility and sulfidability properties of these phases, which were related with the interaction strength between the metal oxides species and the support surface.

Fundamental studies concerning the reduction and sulfidation of the supported phases in HDT catalysts may help in the interpretation of our results. A systematic investigation on the different parameters controlling the activation of $CoMo/\gamma Al_2O_3$ HDS catalysts conducted by Prada Silvy *et al.* [44–49], showed the existence of a direct correlation between the degree of sulfidation of the molybdenum supported species and the catalytic activity for the HDS of thiophene and HYD of cyclohexane. The authors observed that the degree of sulfidation of molybdenum oxide supported species depends on the nature of the sulfiding agent, the reduction and sulfidation temperature and the activation procedure employed [43, 44, 46–48]. Increasing the pretreatment temperature gradually from 300 °C to 400 °C caused a progressive increase of the catalytic activity as well as the degree of sulfidation of the catalyst. The prereduction of the catalyst at $T > 400$ °C affected the degree of sulfidation of the molybdenum species and the catalysts resulted less active for both HDS and HYD reactions [46–49]. It was demonstrated that the behavior of the hydrotreating catalyst in the activation constitutes a typical example of a coupling effect; that is to say, the sulfidation promotes the reduction and the reduction when that occurs simultaneously with the sulfidation, promotes the latter [43, 44].

As mentioned above, another key parameter influencing the reduction and sulfidation of HDT catalysts is the interaction between Mo (W) and the catalyst support. The reduction and sulfidation of $NiW/\gamma Al_2O_3$ proceeds at a lower rate than $CoMo/\gamma Al_2O_3$ or $NiMo/\gamma Al_2O_3$ catalysts. These results were attributed to the relatively strong W–O–Al and W–O bonds [19]. The calcination and sulfidation temperature determined to a large extent the final degree of tungsten sulfidation [20, 50–52]. Ramirez and Gutierrez-Alejandre [8] observed that the incorporation of TiO_2 into the γAl_2O_3 enhances the reducibility and sulfidability properties of tungsten oxide phases due to a reduced interaction with the support surface. The degree of reducibility, as determined by the H_2 consumption, increased progressively with the increasing TiO_2 concentration in the sample. By decreasing the interaction between γ-alumina support with TiO_2 resulted in an easier sulfidation of tungsten at a lower temperature. Cruz-Perez *et al.* [30], using Raman, DRS and XPS techniques of analysis, investigated the interactions between Ni and W in both oxidized and sulfided states in TiO_2–γAl_2O_3 supported catalysts and their effects on HDS reaction of dibenzothiophene. In this study, two NiW/TiO_2–γAl_2O_3 catalysts were prepared by pore filling impregnation method at pH = 4 and pH = 9, respectively. In both cases, $Ni^{2+}W_{12}O_{40}^{6-}$ supported species were observed. The TiO_2–Al_2O_3 isoelectric point (IEP = 6.0) caused a polymerization from WO_4^{2-} monomers at solution pH = 9 onto supported $W_{12}O_{40}^{8-}$. When the solids were calcined, $Ni^{2+}W_{12}O_{40}^{6-}$ + WO_3 and Ni^{2+}/WO_4^{2-} supported species were identified for the solids synthesized at pH = 9 and pH = 4, respectively. For the catalyst prepared at solution pH = 4, the oxide precursor underwent a more efficient sulfidation which led to a higher catalytic activity in HDS.

One may suggest that the differences in catalytic behavior observed between the $NiW/\gamma Al_2O_3$ and NiW/TiO_2–γAl_2O_3 catalysts are the result of an improvement in textural properties, metallic dispersion and surface acidity as well as greater efficiency in the sulfidation of the catalyst. XPS and sulfur content analysis of both $NiW/\gamma Al_2O_3$ and NiW/TiO_2–γAl_2O_3 sulfided catalysts could help to confirm our interpretations.

4.4 Role of ruthenium in promoting the activity properties of $NiWRu/TiO_2$–γAl_2O_3 catalysts

In this section, we will discuss the role that ruthenium plays in combination with the NiW bimetallic systems on improving the catalytic activities for the hydrogenolysis and hydrogenation reactions. We will also try to explain the activity results of the different prepared catalysts on the basis of two theoretical models proposed in the literature that deal with the origin of the catalytic synergy for the hydrogenolysis and hydrogenation reactions between Co(Ni) and Mo(W) sulfides in HDT catalysts.

For this purpose, we prepared two $NiWRu/TiO_2$–γAl_2O_3 catalysts where ruthenium was supported following two different procedures. The first, by co-impregnation with nickel, and in the second, by doping the NiW/TiO_2–γAl_2O_3 catalyst. Both catalysts showed higher catalytic activity than the NiW/TiO_2–γAl_2O_3 catalyst. However, the catalyst prepared by Ni and Ru co-impregnation resulted to be the most active for all the investigated reactions. From these experiments, the promoter effect of ruthenium on improving the catalytic activities for HDS and HDA reactions result evident. However, these benefits depend on the ruthenium incorporation method employed in the preparation of the catalyst. On the other hand, the increase in surface acidity together with the increase in the hydrogenation capacity of the catalyst, due to the incorporation of titanium in the alumina and the promoting effect of ruthenium, produced an increase in the conversion levels for the reactions HDN and MHCK.

To explain the observed differences in catalytic behavior between the $NiW/\gamma Al_2O_3$, NiW/TiO_2–γAl_2O_3 and $NiWRu/TiO_2$–γAl_2O_3 catalysts, it is essential to do a review of the literature in order to identify the different Ni, W and Ru sulfide species formed after the catalyst activation step and their respective intrinsic activities. We will mention below some relevant works published on this topic where both unsupported and supported metal sulfides were used. Let us begin by describing the main findings obtained in those experiments performed with unsupported metal sulfides, and then with supported metals.

One of the most promising research and development works for reaching new regulations related to the sulfur and aromatic content of diesel is the use of noble metals in combination with Ni (Co) and Mo/W bimetallic systems. The selection of these metals was based on results published by Harris and Chianelli [53, 54] and Eijsbouts *et al.* [55]

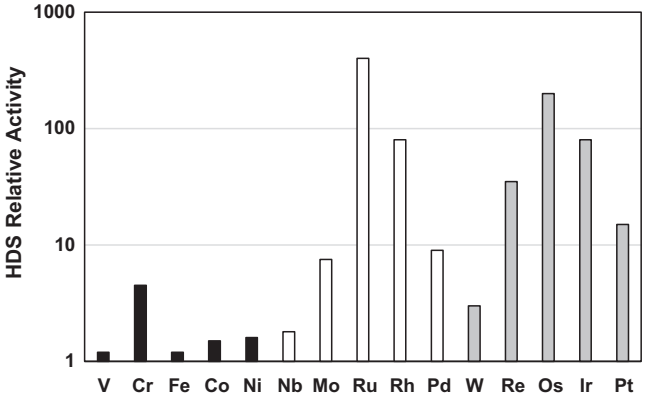

Fig. 6. HDS relative activity for different transition metal sulfides (Harris and Chianelli [53, 54])

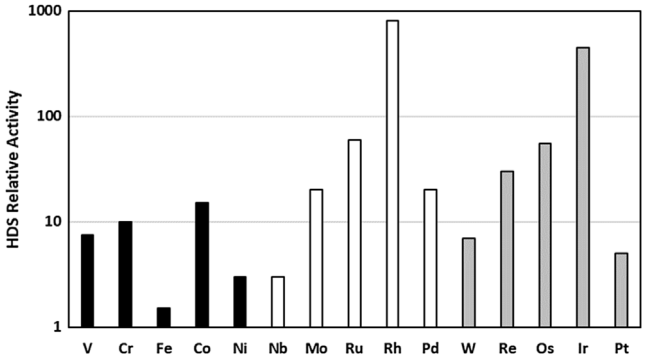

Fig. 7. HDS relative activity for different transition metal sulfides (Ledoux *et al.* [24, 25])

who have found interesting correlations between the HDS activity of Dibenzothiophene (DBT) and the HDN reactions of quinoline [56]. Zdrazil [57], classified different transition metal sulfides according to their selectivity in HDS-HYD and HDS-HDN reactions [24]. This is an important factor to consider at the moment for choosing a commercial HDT or HCK catalyst. A typical "volcano" plot was observed between the intrinsic activity for the HDS of DBT and the periodic table position of groups VI and VIII transition metals bulk sulfides [53, 54].

Figure 6 is a representation of the results obtained by Harris and Chianelli showing the actual activities in HDS as a function of the location of the different metal transition sulfides belonging to groups VI and VIII of the periodic table of the elements. The black, white and gray bars represent the elements located on lines I, II and III, respectively. Significant differences can be observed between the relative activities in HDS between the different metal sulfides located in each line. For the HDS reaction of DBT, ruthenium sulfide was found to be the most active followed by osmium, rhenium and iridium sulfides.

Few years later, Ledoux *et al.* [23] and Chianelli *et al.* [24] carried out a similar study than Harris and Chianelli but in this case, a very low metal sulfide loading was dispersed on an activated charcoal. By determining the HDS activity for thiophene at low level of conversion, Ledoux found that the maximum catalytic activity was observed rhodium followed by iridium, ruthenium and osmium sulfides (Fig. 7). In this case, the relative activities of the cobalt, molybdenum and palladium sulphides significantly increased. The desulfurization reaction of dibenzothiophene can occur through two different mechanisms. Via hydrogenolysis to produce biphenyl or via hydrogenation producing tetrahydrodibenzothiophene as an intermediate compound and then hydrogenolysis to produce cyclohexylbenzene. In the case of hydrodesulfurization of thiophene, the reaction proceeds via hydrogenolysis of the C–S bond. These differences in reaction mechanisms between thiophene and dibenzothiophene, could explain the catalytic behavior of transition metal sulfides for HDT and HYD reactions.

Chianelli *et al.* [24], concluded that the catalytic activity and selectivity of the transition metal sulfides arises from the electronic and structural properties of the sulfides themselves. Isotropic and anisotropic character of the metal sulfide crystal structure, the metal-sulfur bond energy that was related to the heat of formation of the metal sulfide and the sulfur vacancies are also important other factors that were correlated with the catalytic properties of the transition metal sulfide catalysts.

Vrinat *et al.* [25], investigated the catalytic properties in HYD of biphenyl and the HDS of thiophene of a series of ruthenium sulfide solid solution $Me_xRu_{1-x}S_2$ (Me = Fe, Co or Ni). These solid solutions were prepared by sulfidation of co-precipitated Me–Ru hydroxides in H_2S at 400 °C and at 800 °C. The authors observed large differences in conversion levels among the $Me_xRu_{1-x}S_2$ prepared catalysts. The catalytic activity properties strongly depend on the nature of the metal associated with ruthenium and its atomic composition in the mixed sulfide. The $Ni_xRu_{1-x}S_2$ showed remarkable HDS and HYD activity properties, almost twice the activity of RuS_2. The $Co_xRu_{1-x}S_2$ solid solution also showed high activity in HDS but lower activity in HYD while, $Fe_xRu_{1-x}S_2$ showed poor catalytic properties for both hydrogenolysis and hydrogenation reactions. For the HDS reaction of thiophene, the activity of the $Me_xRu_{1-x}S_2$ compounds varied as follow:

$$Fe_{0.8}Ru_{0.2}S_2 << RuS_2 < Co_{0.8}Ru_{0.2}S_2 < Ni_{0.8}Ru_{0.2}S_2 < Ni_{0.6}Ru_{0.4}S_2$$

while, for the HYD reaction of biphenyl the observed sequence was:

$$Fe_{0.8}Ru_{0.2}S_2 << Co_{0.8}Ru_{0.2}S_2 << RuS_2 < Ni_{0.8}Ru_{0.2}S_2 = Ni_{0.6}Ru_{0.4}S_2.$$

In the same work, the activity properties of the $Me_xRu_{1-x}S_2$ solid solutions were compared with MoS_2, and the "MeMoS" mixed phases. These catalysts were prepared by the homogeneous sulfide precipitation method developed by Candia *et al.* [58]. In typical HDT catalysts, an optimum conversion was observed for a Co(Ni)/[Co(Ni)+Mo(W)] molar ratio between 0.25 and 0.40, no matter which catalyst support,

pair of active sulfides were used and what type of reaction. In this case, the intrinsic activity in HDS varied according to the following sequence:

$$FeMoS << MoS_2 << CoMoS < NiMoS < RuS_2 << Ni_{0.6}Ru_{0.4}S_2$$

while, the intrinsic activity in HYD varied as follow:

$$FeMoS << MoS_2 < CoMoS << RuS_2 < NiMoS << Ni_{0.6}Ru_{0.4}S_2.$$

The catalytic behavior of both $Me_xRu_{1-x}S_2$ compounds were explained by the existence of a promoting effect between M*e*–Ru pair sites, whose electronics and activity properties were related to the nature of the components.

To explain the catalytic synergy between M*e*MoS sulfides in hydrotreating catalysts about 17 theoretical models have been proposed in the literature. The main debate currently rests on two of these theories, the so-called CoMoS, NiMoS, NiWS phase proposed by Topsøe *et al.* [59, 60] and the synergy by contact - remote control mechanism, proposed by Delmon [61–63].

From Mossbauer spectroscopy studies carried out with unsupported and supported Co and Mo sulfides catalysts, Topsøe proposed that the active centers in HDS are due to a CoMoS-like structure that consist on cobalt atoms inserted at various places on the edges of MoS_2 crystallites sheets and present a specific coordination. A direct correlation between the amount of promoter atoms present in the CoMoS phase and the activity in HDS reactions was established [64]. Two types of CoMoS phases were identified. CoMoS type I phase, which consists of a highly dispersed monolayer structure and it is partially sulfided. Some Mo (W)–O–Al bonds were identified by FTIR (NO) and XPS analysis, the interaction with the support is relatively strong. The CoMoS type II phase which consists of a less dispersed stacked structure and is completely sulfided. Its interaction with the catalyst support is weak. The CoMoS type II phase showed a higher activity in the HDS of thiophene and quinoline HDN than type I. However, NiMoS Type I phase resulted more active for the DBT HDS reactions. The active phase of supported NiW sulfide catalysts was found to be similar to the so-called CoMoS and NiMoS phases in supported on γAl_2O_3 activated catalysts [65]. For the NiW/γAl_2O_3 catalyst, two types of 'NiWS' phases were distinguished by Hensen *et al.* [20] and Breysse *et al.* [66]. They reported that a NiWOS type I phase with some residual oxygen linkages were formed after low temperature sulfidation exhibiting high hydrogenation activity, whereas higher sulfidation temperatures resulted in the formation of a NiWS type II phase with a high HDS activity.

The synergy by contact–remote control mechanism was proposed by Delmon from experiments conducted with mechanical mixtures from Group VI and Group VIII sulfides [61–63]. This model proposes that the activity and selectivity are related to the cooperation between the MoS_2 and Co_9S_8 separated phases, and that synergy by contact between these two phases occurs during the catalytic reaction. A remote control of the active phase located at the edge planes of the hexagonal MoS_2 (or WS_2) crystallites is exerted by the second phase which is able to activate hydrogen. Noble metals, cobalt or nickel sulfides have the ability to efficiently activate hydrogen molecules by dissociation of their bonds and then, these activated (H^*_{so}) species are transferred to the MoS_2 (WS_2) surface through a spill-over mechanism. MoS_2 (WS_2) phase would carry the active sites for the HDS and HYD reactions. The main role of activated hydrogen species is to create or regenerate active catalytic sites but they do not directly participate in hydrogenolysis or hydrogenation reactions. The slightly reduced sites in the MoS_2 crystallites would be responsible for the HYD reactions while, the strongly reduced centers would the responsible for the HDS reactions.

The main controversy in the literature is due to experiments conducted by several research groups whose catalytic activity results were explained either by the CoMoS phase model or by the synergy by contact–remote control mechanism. Below we will mention some published works that deal with the characterization of the structure of the active phases in supported metal sulfides catalysts and their stability under HDT reaction conditions. A schematic representation proposed for NiW based catalysts according to Topsøe and Delmon theoretical models is shown in Figures 8a and 8b, respectively.

Prada Silvy and Ladriere [44, 49], using the Mossbauer Emission Spectroscopy technique, investigated the effect of the sulfidation temperature on the structure and composition of the cobalt supported phases in a CoMo/γAl_2O_3 catalyst doped with Co^{57} isotopes. The pretreatments were conducted using a 5 v% H_2S in H_2 gas mixture at atmospheric pressure and at temperatures between 400 and 800 °C. Although activation temperatures greater than 400 °C are not common in practice, however, this type of experiments could help to understand some possible transformations that could occur in the catalyst during a long reactor operation cycle. In the temperature range 400–650 °C, it was observed that the cobalt atoms from the CoMoS phase begin to segregate to produce Co_9S_8 and CoS_{1-x} and simultaneously, a decrease in the $CoAl_2O_4$ phase composition was produced. Despite these changes in structure and composition of the supported cobalt phases, both HDS and HYD catalytic activities remained constant. Vrinat *et al.* [25], and Breysse *et al.* [66], observed segregation of the cobalt atoms in the CoMoS phase after a reduction treatment in H_2 or the catalytic reaction at $T \geq 400$ °C. Similar changes were observed at high sulfidation temperatures found by Topsøe's group [67] when a CoMo/γAl_2O_3 catalyst was submitted to reaction for 19 h in the presence of a vacuum gas oil at 350 °C and a total pressure of 10 MPa.

Candia *et al.* [58] have found that the stability of the CoMoS phase strongly depend on the Co/Mo atomic ratio. For instance, for a Co/Mo ratio = 0.09, the CoMoS phase remained stable at sulfidation temperatures from 400 °C to 700 °C, whereas for a Co/Mo ratio = 0.27, the Co atoms were observed to segregate out of CoMoS phase to produce Co_9S_8. Industrial HDT catalysts have a Co (Ni)/(Co (Ni) + Mo (W)) ratio of about 0.30 or Co(Ni)/Mo(W) atomic ratio = 0.43. This Co/Mo atomic ratio is higher than the CoMoS phase synthesized by Candia, in which would

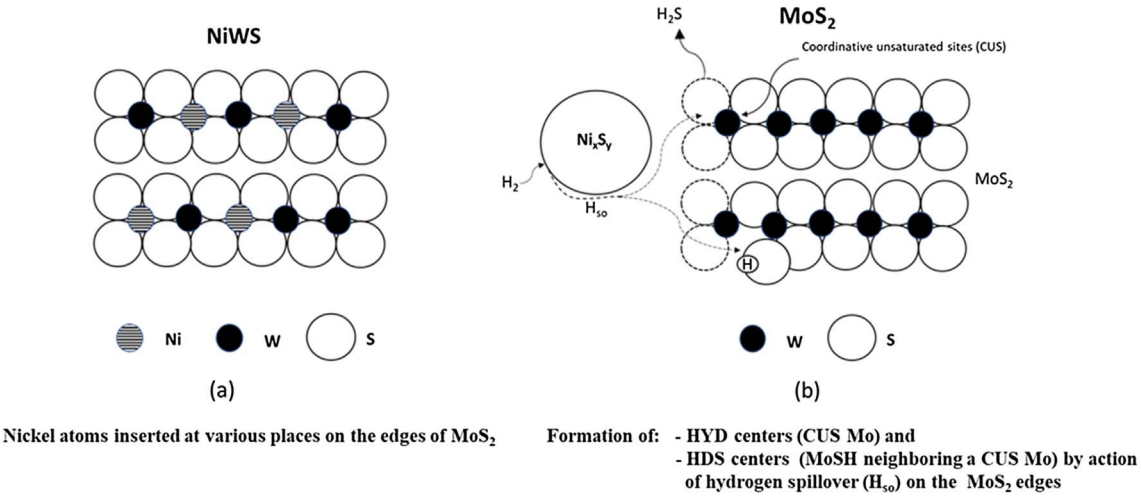

Fig. 8. Schematic representation proposed for NiWS phase and synergy by contact–remote control theoretical models.

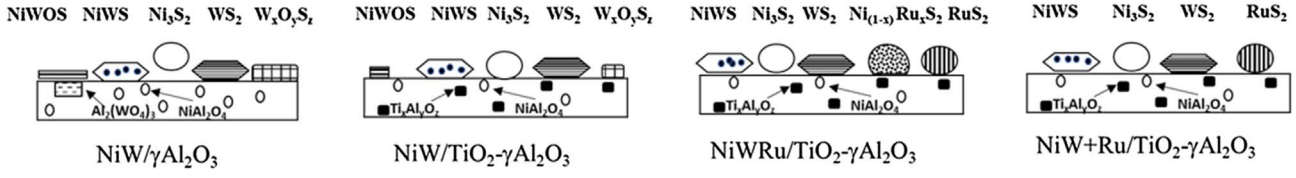

Fig. 9. Schematic representation of the different Ni, W, Ru and Ti supported phases in the different prepared HDT catalysts after sulfidation.

expect this phase to be less stable under typical HDT or HCK process conditions. As a consequence of the metastability of CoMoS phase, it is normal that this phase decomposes to produce separated Co_9S_8 and MoS_2 slightly doped with Co phases under long term HDS operation conditions. The catalytic synergy between the CoMoS phase slightly doped with cobalt atoms and Co_9S_8 is much greater than that existing between the Co_9S_8 and MoS_2 phases [39, 44]. Our results were confirmed by Karroua *et al.* [68] who observed that the activity of the mechanical mixtures of "CoMoS" and Co_9S_8 is almost double that obtained by adding contributions from the separate components.

Taking into account the works published in the literature on the characterization of the Co (Ni) and Mo (W) supported phases in HDT catalysts using different techniques of analysis, Figure 9 represents schematically the different Ni, W, Ru and Ti phases present in $NiW/\gamma Al_2O_3$, $NiW/TiO_2\text{–}\gamma Al_2O_3$, $NiWRu/TiO_2\text{–}\gamma Al_2O_3$ and $NiW+Ru/TiO_2\text{–}\gamma Al_2O_3$ sulfided catalysts.

In the $NiW/\gamma Al_2O_3$ catalyst, tungsten atoms can be found associated with the alumina in the form of stable aluminum tungstate like phase ($Al_2(WO_4)_3$) and on the surface in a partially or totally sulfidized state distributed in the following phases: NiWOS, $W_xO_yS_z$, NiWS and WS_2. Nickel atoms can form a spinel-like structure with the alumina ($NiAl_2O_4$), and be located on the surface forming isolated Ni_3S_2 species or in a mixed phase with tungsten sulfides.

As discussed in Section 4.1, incorporation of titanium at the tetrahedral sites of the alumina network results in the formation of a $TiAl_2O_5$-type compound causing a decrease in $NiAl_2O_4$ species. We could also suggest that the role of titanium is to prevent the formation of tungsten species associated with the alumina. Other works indicated that titanium facilitates the reduction – sulfidation properties of the tungsten oxides species on the surface due to the fact that it decreases its interaction strength with alumina. According to these experimental results, for the $NiW/TiO_2\text{–}\gamma Al_2O_3$ catalyst, a higher WS_2 and NiWS surface composition would be expected due to a more efficient sulfidation of the tungsten species at the activation temperature. Isolated Ni_3S_2 species are also present on the surface of the $NiW/TiO_2\text{–}\gamma Al_2O_3$ catalyst.

For both $NiWRu/TiO_2\text{–}\gamma Al_2O_3$ catalysts, the presence of ruthenium on the surface would further facilitate the reduction-sulfidation reaction of tungsten oxide species at lower activation temperature. It is well known that noble metals can easily dissociate H_2 molecules to produce 2H* activated species. These compounds are more efficient reducing agents than other transition metals. It would then be expected that in both catalysts, the tungsten would be totally sulfided forming WS_2 and NiWS phases. In the $NiWRu/TiO_2\text{–}\gamma Al_2O_3$ catalyst, which was prepared by Ni and Ru co-impregnation, the nickel atoms could be distributed in different phases: i) a small amount associated with the alumina in the form of nickel aluminate, ii) as isolated Ni_3S_2 species and iii) forming with W and Ru

mixed sulfides phases. The formation of a $Me_xRu_{1-x}S_2$ mixed phase comes from experiments carried out by Vrinat *et al.* [25] and Passaretti *et al.* [69]. However, it should be pointed out that these compounds were synthesized at a high sulfidation temperature and little is known about their stability under reaction conditions. The $Co_xRu_{1-x}S_2$ compounds have been reported to decompose into their respective individual metal sulfides under typical HDT conditions [69–71].

Ruthenium atoms can also be in the form of RuS_2. One could speculate the possibility of some Ru atoms that could be found doping the WS_2 and NiWS phases, having some implications on the intrinsic activity of these phases. In the case of NiW + Ru/TiO_2–γAl_2O_3 catalyst, ruthenium would only be expected to be as RuS_2. After impregnation step with ruthenium, the catalyst was dried at 180 °C to remove water and chlorides and then directly sulfided.

It now remains to explain the activity of $NiWRu/TiO_2$–γAl_2O_3 catalysts based on the theoretical models mentioned earlier. According to the model proposed by Topsøe, the CoMoS phase is a family of sulfided Co (Ni) and Mo (W) compounds which have variable composition of the promoter atoms located at different positions on the edge surface of the MoS_2 crystallites. Studies carried out on the stability of the CoMoS phase at high sulfidation temperatures, after reduction treatment in the presence of hydrogen and after having subjected the compound under HDT conditions, revealed that the promoter atoms begin to segregate out to form nanoparticles of highly dispersed cobalt sulfide. However, a certain amount of cobalt remained attached to the lateral surface of the MoS_2. This suggests that not all sites occupied by the promoter atoms at the edge plane of MoS_2 (WS_2) are energetically equivalent, since the amount of Co (Ni) segregated will depend on the interaction forces at the sites where they are located (corners of edges sites), on the temperature and on the Co (Ni)/Mo(W) atomic ratio in the compound.

Given that, there was an established correlation between the number of cobalt atoms in the CoMoS phase and the catalytic activity, it would be expected that the initial activity of the catalyst is high and as the cobalt begins to segregate due to its instability, the conversion to HDS will decrease progressively. In a hydrotreating reactor, the catalyst can last several months in operation, depending on the severity of the process. Under conditions of high pressure in hydrogen and temperature, the segregation process of the Co(Ni) atoms would be favored. This process of segregation of the Co (Ni) atoms could also be accelerated if the catalyst contains noble metals in its formulation due to its ability to produce H* activated species which are highly reactive. The CoMo, NiMoS or NiWS phase that remains stable would have a low Co/Mo ratio. However, the level of HDS and HYD conversion remained constant.

Based on these interpretations, the catalytic activity of a commercial HDT catalyst cannot be explained solely through the CoMoS phase model due to its metastability under process conditions. According to the model proposed by Delmon, the catalytic synergy in HDS depends on the number and quality of the contact between the Co_9S_8 (Ni_3S_2) and MoS_2 (WS_2) phases. The formation of Co_9S_8 nanoparticles from the cobalt segregation associated with the CoMoS phase and their proximity to this compound, would increase the synergy effect between both phases. Co_9S_8 (Ni_3S_2) nanoparticles have a larger surface area than bulk sulfide compounds, indicating its more effectiveness in dissociating hydrogen molecules to accelerate the creation or regeneration of active centers. This effect compensates for the loss of catalytic activity due to the decrease in the number of Co (Ni) atoms associated with the CoMoS phase (NiMoS or NiWS).

Based on the above discussion, it could be proposed that a dual mechanism would satisfactorily explain the catalytic activity of hydrotreating catalysts. The synergy by contact-remote control mechanism between the CoMoS phase (NiMoS or NiWS), having a low Co/Mo (Ni/Mo or Ni/W) atomic ratio, and the Co_9S_8 phase (Ni_3S_2). The combination of both models would allow to understand the physico-chemical transformations that may occur in the catalyst at the beginning and during the long reactor operation cycle. It would then be expected that the initial activity of the catalyst could be associated with a greater contribution of the CoMoS phase (NiMoS or NiWS) and as the promoter atoms begin to segregate to form new individual metal sulfides phases, the synergy by contact–remote control mechanism begins to dominate the catalytic process thus, the catalytic reaction begins to stabilize. The promoter atoms (Ni and Ru) in the $NiWRu/TiO_2$–γAl_2O_3 catalyst can influence the reduction-sulfidation properties of the tungsten oxides supported phases during the catalyst activation. It is well known that noble metals can easily dissociate H_2 molecules to create H^*_{so} activated species which are highly effective reducing agents. The efficiency in the activation of the hydrotreating catalysts is determined by a coupling effect between both reduction-sulfidation reactions. Accordingly, the $NiWRu/TiO_2$–γAl_2O_3 catalyst would be expected to exhibit a more complete sulfidation than the NiW/TiO_2–γAl_2O_3 catalyst, as illustrated in Figure 10. On the other hand, as the number of H^*_{so} activated species due to presence of Ru in the catalyst, they could accelerate both, the process of creation or regeneration of active sites and the segregation of the promoter atoms of the NiWS phase. The dual mechanism concept for the $NiWRu/TiO_2$–γAl_2O_3 catalyst is represented in Figure 10.

It was also observed that the $NiWRu/TiO_2$–γAl_2O_3 catalyst showed sulfur resistance properties when it was subjected to different H_2S partial pressures between 0 and 10 psi. These results are shown in Figure 11.

It is clearly evident that the $NiWRu/TiO_2$–γAl_2O_3 is less effected by increase in H_2S partial pressure compared to NiW/TiO_2–γAl_2O_3 catalyst.

This behavior was also observed for $Co_{(1-x)}Ru_xS_2$ mixed phase [72]. One can speculate that the efficiency of individual metal sulfides in creating or regenerating active centers is related to the thio-resistance properties of the catalyst. This efficiency will depend on the surface composition of both Ni_3S_2 and RuS_2, state of dispersion and quality of contact with the NiWS and WS_2 phases.

According to the aforementioned works, ruthenium could form a mixed phase with Ni, ($Ni_{(1-x)}Ru_xS_2$). This compound showed a high intrinsic activity in HDS.

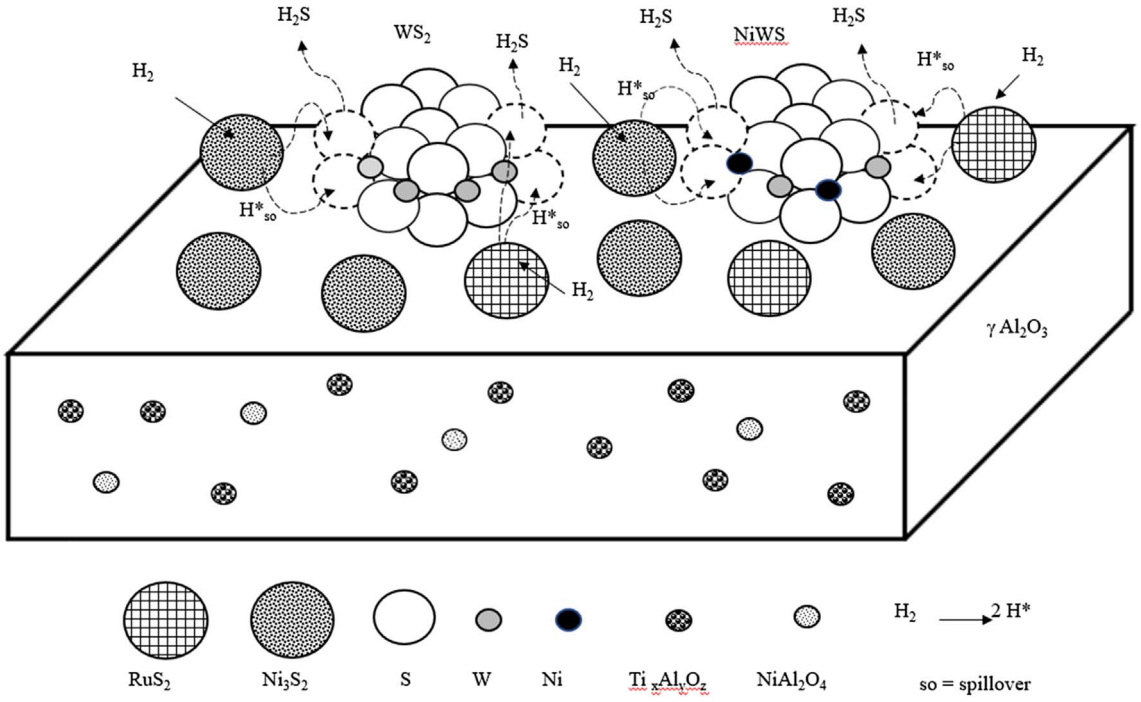

Fig. 10. Representation of the dual mechanism concept.

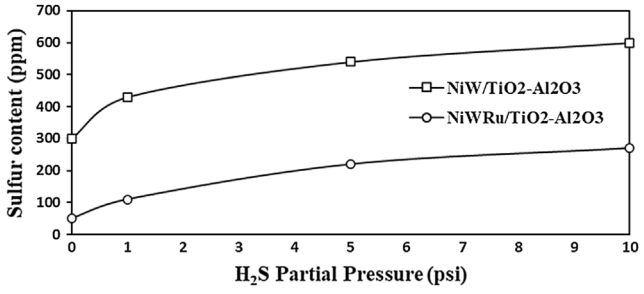

Fig. 11. Sulfur content in diesel fraction at different H_2S partial pressures.

However, they could be decomposed into their individual metal sulfide species during at high pressure and temperature conditions. Although $Ni_{(1-x)}Ru_xS_2$ compound was synthesized at high temperature, its formation of in the $NiWRu/TiO_2–\gamma Al_2O_3$ catalyst prepared by co-impregnation of Ni and Ru cannot be discarded.

4.5 Ultra-low sulfur and aromatic compounds in Diesel

In this set of experiments, a pretreated heavy gas oil blend containing light cycle oil, heavy coker gasoil and heavy vacuum gasoil in the 30%, 40% and 30 v% proportions, respectively, was employed. This HGO feedstock contained 1300 ppm S, 300 ppm N, 55 v% aromatic and 100 v% of 250–500 °C distillation fraction range. The reactor operation conditions were as following: $T = 360$ °C, $P = 1200$ psig, $H_2/HC = 1000$ v/v and LHSV = 0.50 h^{-1}. The different fractions were separated by distillation to conduct S, N and aromatic content analysis and other properties.

Table 5 shows the properties of the diesel fractions obtained with both $NiWRu/TiO_2–\gamma Al_2O_3$ and $NiW/TiO_2–\gamma Al_2O_3$ catalysts. The 370 °C$^+$ fraction was about 30 v% while the Diesel fraction represents about 55 v% of the hydrotreated product. At high H_2 partial pressure, the HDS, HDN and HDA conversion dramatically increases when ruthenium is present in the $NiW/TiO_2–\gamma Al_2O_3$ catalyst formulation.

Ultra-Low Sulfur Diesel having very low nitrogen and aromatic content and high cetane index was obtained. The observed differences in cloud point, associated with the amount of isoparaffinic material in the Diesel fraction is particularly noteworthy.

High HDS, HDN and HDA activities were also observed when doping $NiW/TiO_2–\gamma Al_2O_3$ catalyst with palladium instead ruthenium. In this case, a product containing about 22 ppm S, 2 ppm N and 15 v% aromatics was obtained using a VGO + LGO hydrotreated feedstock (40 v%/60 v%). In these experiments, the reactor was operated at $T = 370$ °C, $P = 12.4$ MPa, LHSV = 0.5 h^{-1} and H_2/hydrocarbon ratio = 800 Nm^3/m^3. Comparison between $NiWRu/TiO_2–\gamma Al_2O_3$ and $NiWPd/TiO_2–\gamma Al_2O_3$ catalyst systems will be published elsewhere [73].

5 Conclusion

The conclusions that emerge from this work are the following:

We have successfully demonstrated the selective conversion of heavy gasoil into middle distillates fuels that

meet with the ultra-low sulfur and aromatic standards by using a NiWRu/TiO_2–γAl_2O_3 based catalyst under typical hydrotreating operating conditions.

The coprecipitation of titanium and aluminum hydroxides produced a catalyst support having greater surface area, pore volume, surface acidity and metallic surface dispersion than alumina.

The NiW/TiO_2–γAl_2O_3 and NiWRu/TiO_2–γAl_2O_3 catalysts exhibited a greater surface dispersion of the supported nickel and tungsten species compared to the reference NiW/γAl_2O_3 material.

The promoter effect of ruthenium on the NiW bimetallic system caused a strong increase in both HDS and HDA activities. The HDN and HCK reactions were also seen favored by the increase in the hydrogenation capacity and the surface acidity of the catalyst.

The highest conversion levels for all investigated reactions were obtained when the NiWRu/TiO_2–γAl_2O_3 catalyst was prepared by co-impregnation of Ni and Ru. This catalyst showed sulfur tolerance properties when the reaction was conducted in the presence of different H_2S partial pressures.

The catalytic behavior of the NiWRu/TiO_2–γAl_2O_3 catalyst was explained by the existence of a promoting effect between separated Ni and Ru sulfides species and the NiWS phase (dual mechanism).

Acknowledgments. Dr. Ricardo Prada Silvy wants to dedicate this work in memory to professors Dr. Bernard Delmon from the Université Catholique de Louvain (Belgium) and Dr. Lyezer Katan from the Central University of Venezuela who had a great influence on his professional career.

References

1 Stanislaus A., Marafi A., Rana M.S. (2010) Recent advances in the science and technology of ultra low sulfur diesel (ULSD) production, *Catal. Today* **153**, 1–68.
2 Diaz de Leon J.N., Kumar C.R., Antunez-Garcia J., Fuentes-Moyado S. (2019) Recent insights in transition metal sulfide hydrodesulfurization catalysts for the production of ultra low sulfur diesel: A short review, *Catalysts* **9**, 87, 1–26.
3 Fujikawa T. (2006) Highly active CoMo HDS catalyst for the production of clean diesel fuels, *Catal. Surv. Asia* **10**, 89–97.
4 Asian Clean Fuel Association, CAI-Asia (2011) *A Road Map for cleaner Fuels and vehicles in Asia*, Factsheet 17, September 2011.
5 Peckham J. (2006) Road Map for Asia' Pushes Cleaner Fuels; "Gradual" desulfurization seen inefficient, *Diesel Fuel News* Jun 5, 10–12.
6 Delmon B. (1993) New technical challenges and recent advances in hydrotreatment catalysis. A crucial updating review, *Catal. Lett.* **22**, 1–32.
7 Wan G., Duan A., Zhang Y., Zhao Z., Jiang G., Zhang D., Li J., Chung K. (2010) NiW/AMBT catalysts for the production of ultra-low sulfur diesel, *Catal. Today* **23**, 521–529.
8 Ramirez J., Gutierrez-Alejandre A. (1998) Relationship between hydrodesulfurization activity and morphological and structural changes in NiW hydrotreating catalysts supported on Al_2O_3-TiO_2 mixed oxides, *Catal. Today* **43**, 123–133.
9 Luck F. (1991) A review of support effects on the activity and selectivity of hydrotreating catalysts, *Bull. Soc. Chim. Belg.* **100/n°**, 11–12, 781–800.
10 Tanaka H., Boulinguiez M., Vrinat M. (1996) Hydrodesulfurization of thiophene, dibenzothiophene and gas oil on various Co-Mo /TiO_2-Al_2O_3 catalysts, *Catal. Today* **29**, 209–213.
11 Vasquez-Garrido I., Lopez-Benitez A., Berhault G., Guevara-Lara A. (2019) Effect of support on the acidity of NiMo/Al_2O_3-MgO and NiMo/TiO_2-Al_2O_3 catalysts and on the resulting competitive hydrodesulfurization/hydrodenitrogenation reactions, *Fuel* **236**, 55–64.
12 Olguin E., Vrinat M., Cedeno L., Ramirez J., Borque M., Lopez-Agudo A. (1997) The use of TiO_2-Al_2O_3 binary oxides as supports for Mo-based catalysts in hydrodesulfurization of thiophene and dibenzothiophene, *Appl. Catal. A* **165**, 1–13.
13 Castillo-Villalon P., Ramirez J., Cuevas R., Vasquez P., Castanedas R. (2015) Influence of the support on the catalytic performance of Mo, CoMo, and NiMo catalysts supported on Al_2O_3 and TiO_2 during the HDS of thiophene, dibenzothiophene, or 4,6-dimethyldibenzothiophene, *Catal. Today* **259**, 40–149.
14 Wan G., Duan A., Zhao Z., Jiang G., Zhang D., Li R., Dou T., Chung K. (2009) Al_2O_3-TiO_2/Al_2O_3-TiO_2-SiO_2 composite supported bimetallic Pt-Pd catalysts for the hydrodearomatization and hydrodesulfurization of diesel fuel, *Energy Fuels* **23**, 81–85.
15 Prada Silvy R., Galiasso R., Romero Y., Reyes E., Muñoz R. (1993) *US Patent 5,229,347.*
16 Grange P., Vanhaeren X. (1997) Hydrotreating catalysts, an old story with new challenges, *Catal. Today* **36**, 375–391.
17 Prada Silvy R. (2019) Scale-up of a NiMoP/γAl_2O_3 catalyst for the hydrotreating and mild hydrocracking of heavy gasoil, *Oil Gas Sci. Technol. – Rev. IFP Energies nouvelles* **74**, 22.
18 Yoshinaka S., Segawa K. (1998) Hydrodesulfurization of dibenzothiophenes over molybdenum catalyst supported on TiO_2-Al_2O_3, *Catal. Today* **45**, 293–298.
19 Zotin J.L., Cattenot M., Portefaix J.L., Breysse M. (1995) Conversion of nitrogen containing molecules in the presence of a mixture of nickel molybdenum supported on alumina and ruthenium sulfide dispersed in a KY zeolite, *Bull. Soc. Chim. Belg.* **104**, 4–5, 213–218.
20 Hensen E.J.M., Van der Meer Y., Van Veen J.A.R., Niemantsverdriet J.W. (2007) Insight into the formation of the active phases in supported NiW hydrotreating catalysts, *Appl. Catal., A* **322**, 16–32.
21 Obeso-Estrella R., Fierro J.L.G., Diaz de Leon J.N., Fuentes S., Alonso-Nunez G., Lugo-Medina E., Pawelec B., Zepeda T.A. (2018) Effect of partial Mo substitution by W on HDS activity using sulfide CoMoW/Al_2O_3 - TiO_2 catalysts, *Fuel* **233**, 644–657.
22 Breysse M., Djega-Mariadassous G., Pessayre S., Geantet C., Vrinat M., Perot G., Lemaire M. (2003) Deep desulfurization: reactions, catalysts and technological challenges, *Catal. Today* **84**, 129–138.
23 Ledoux M.J., Michaux O., Agostini G., Panissod P. (1986) The influence of sulfide structures on the hydrodesulfurization activity of carbon-supported catalysts, *J. Catal.* **102**, 275.
24 Chianelli R.R., Daage M., Ledoux M.J. (1994) Fundamental studies of transition-metal sulfide catalytic materials, *Adv. Catal.* **40**, 177–232.

25 Vrinat M., Lacroix M., Breysse M., Mosoni L., Roubin M. (1989) Catalytic properties in hydrogenation and hydrodesulphurization reactions of ruthenium sulphide solid solutions containing iron, cobalt or nickel, *Catal. Lett.* **3**, 405–412.

26 Prada Silvy R. (2019) Parameters controlling the scale-up of CoMoP/γ- Al_2O_3 and NiMoP/γAl_2O_3 catalysts for the hydrotreating and mild-hydrocracking of heavy gasoil, *Catal. Today* **338**, 93–99.

27 Maduna Valkaj K., Kaselj I., Smolkovic J., Zrncevic S., Kumar N., Murzin D. (2015) Catalytic wet peroxide oxidation of olive oil mill wastewater over zeolite based catalyst, *Chem. Eng. Trans.* **43**, 853–858.

28 Zhaobin W., Qin X., Xiexian G., Sham E.L., Grange P., Delmon B. (1990) Titania-modified hydrodesulphurization catalysts I. Effect of preparation techniques on morphology and properties of TiO_2-Al_2O_3 carrier, *Appl. Catal* **63**, 305–317.

29 Ramirez J., Ruiz-Ramirez L., Cedeno L., Harle V., Vrinat M., Breysse M. (1993) Titania-alumina mixed oxides as supports for molybdenum hydrotreating catalysts, *Appl. Catal., A* **93**, 163–180.

30 Cruz-Perez A.E., Guevara-Lara A., Morales-Ceron J.P., Alvarez-Hernadez A., de los Reyes J.A., Massin L., Geantet C., Vrinat M. (2011) Ni and W interactions in the oxide and sulfide states on an Al_2O_3-TiO_2 support and their effects on dibenzothiophene hydrodesulfurization, *Catal. Today* **172**, 203–208.

31 Bonsack J.P. (1973) Ion-exchange and surface properties of titania gels from Ti (IV) sulfate solutions, *J. Coll. Interf. Sci.* **44**, 430.

32 Guevara-Lara A., Bacaud R., Vrinat M. (2007) Highly active NiMo/TiO_2-Al_2O_3 catalysts: Influence of the preparation and the activation conditions on the catalytic activity, *Appl. Catal., A* **328**, 99–108.

33 Freudenberg B., Mocellin A. (1988) Aluminum titanate formation by solid-state reaction of coarse Al2O3 and TiO2 powders, *J. Am. Ceram. Soc.* **71**, 22–28.

34 Freudenberg B., Mocellin A. (1990) Aluminium titanate formation by solid state reaction of Al_2O_3 and TiO_2 single crystals, *J. Mater. Sci.* **25**, 3701–3708.

35 Zhou Y., Yin J., Xu H., Xia Y., Liu Z., Li A., Gong Y., Pu L., Yan F., Shi Y. (2010) A $TiAl_2O_5$ nanocrystal charge trap memory device, *Appl. Phys. Lett.* **97**, 143504.

36 Lee M.-H., Feng C.-F., Heine V., Klinowski J. (1997) Distribution of tetrahedral and octahedral A1 sites in gamma alumina, *Chem. Phys. Lett.* **265**, 6, 673–676.

37 Shee D., Deo G., Hirt A.M. (2010) Characterization and reactivity of sol-gel synthetized TiO_2- Al_2O_3 supported vanadium oxide catalysts, *J. Catal.* **273**, 221–228.

38 Li Z., Meng M., You R., Ding T., Li Z. (2012) Superior performance of mesoporous TiO_2-Al_2O_3 supported NSR catalysts with the support synthesized using nonionic and cationic surfactants as Co-templates, *Catal. Lett.* **142**, 1067–1074.

39 Ramos-Galvan C.E., Sandoval-Roble G., Castillo-Mares A., Dominguez J.M. (1997) Comparison of catalytic properties of NiMo/Al_2O_3 with NiMo supported on Al, Ti-pillared clays in HDS of residual oils, *Appl. Catal. A* **150**, 37–52.

40 Gil Llambias F.J., Bouyssieres L., Lopez-Agudo A. (1990) Preparation and characterization by electrophoretic migration of TiO_2-Al_2O_3 catalytic supports, *Appl. Catal.* **65**, 45.

41 Akratopulu K., Kordulis C., Lycourghiotis A. (1990) Effect of temperature on the point of zero charge and surface charge of TiO_2, *J. Chem. Soc. Faraday Trans.* **86**, 3437–3440.

42 Kohler S.D., Ekerdt J.D., Kim D.S., Wachs I.E. (1992) Relationship between structure and point of zero surface charge for molybdenum and tungsten oxides supported on alumina, *Catal. Lett.* **16**, 231.

43 Spanos N., Matralis H.K., Kordulis Ch, Lycourghiotis A. (1992) Molybdenum-oxo species deposited on titania by adsorption: Mechanism of the adsorption and characterization of the calcined samples, *J. Catal.* **136**, 432.

44 Prada Silvy R. (1987) Parameters controlling the activation of CoMo/Al_2O_3 hydrodesulfurization catalysts. *PhD Thesis*, Univ Catholique de Louvain, Belgium.

45 Prada Silvy R., Grange P., Delannay F., Delmon B. (1989) Influence of the nature of the activating molecules on the catalytic activity of cobalt-molybdenum/alumina catalysts, *Appl. Catal.* **46**, 113–129.

46 Prada Silvy R., Delannay F., Delmon B. (1987) Influence of the activation temperature on the degree of sulfidation, dispersion and catalytic activity of Co-Mo/γAl2O3 catalysts, *Indian J. Technol.* **25**, 627.

47 Prada Silvy R., Beuken J.M., Garcia Fierro J.L., Bertrand P., Delmon B. (1986) Surface investigation, by XPS, ISS and IR spectroscopy of adsorbed NO of the structural changes occurring during the reduction of Co-Mo/γAl2O3 catalysts, *Surf. Interface Anal.* **8**, 167.

48 Prada Silvy R., Grange P., Delmon B. (1987) *IV International Symposium on Preparation of Heterogeneous Catalysts*, Louvain-la-Neuve, Belgium, p. 605.

49 Ladriere J., Prada Silvy R. (1988) Mössbauer emission studies of Co-Mo/γAl2O3 hydrodesulfurization catalysts: Effects of reduction and sulfidation treatments, *IX International Conference on Mössbauer Application Hyperfine Interactions* **41**, 653–656.

50 Scheffer B., Mangnus P.J., Moulijn J.A. (1990) A temperature-programmed sulfiding study of NiO/Al_2O_3 catalysts, *J. Catal.* **121**, 18.

51 Van der Vlies A.J., Kishan G., Niemantsverdriet J.W., Prins R., Weber Th (2002) Basic reaction steps in the sulfidation of crystalline tungsten oxides, *J. Phys. Chem. B* **106**, 13, 3449.

52 Van der Vlies A.J., Prins R., Weber Th (2002) Chemical principles of the sulfidation of tungsten oxides, *J. Phys. Chem. B.* **106**, 36, 9277.

53 Harris S., Chianelli R.R. (1983) Periodic effects in catalysis: The relation between trends in catalytic activity and calculated electronic structure of transition-metal sulfides, *Chem. Phys. Lett.* **101**, 603.

54 Harris S., Chianelli R.R. (1984) Catalysis by transition metal sulfides: the relation between calculated electronic trends and HDS activity, *J. Catal.* **86**, 400–412.

55 Eijsbouts S., Dudhakar C., de Beer V.H.J., Prins R. (1988) Periodic trends in the hydrodenitrogenation activity of carbon-supported transition metal sulfide catalysts, *J. Catal.* **109**, 217.

56 Ledoux M.J., Djellouli B. (1989) Hydrodenitrogenation activity and selectivity of well-dispersed transition metal sulfides of the second row on activated carbon, *J. Catal.* **115**, 580–590.

57 Zdrazil M. (1988) Recent advances in catalysis over sulphides, *Catal. Today* **3**, 269–365.

58 Candia R., Clausen B.J., Topsøe H. (1981) On the role of promoter atoms in unsupported hydrodesulfurization catalysts: Influence of preparation methods, *Bull. Soc. Chim. Belg.* **90**, 12, 1225.

59 Topsøe H. (1983) *Surface science and catalysis by non-metals*, Elsevier Science Publishers B.V., Amsterdam, The Netherlands, p. 329.

60 Topsøe H., Clausen B.S., Candia R., Wivel C., Morup S. (1981) In situ Mössbauer emission spectroscopy studies of unsupported and supported sulfided Co-Mo hydrodesulfurization catalysts: Evidence for and nature of a Co-Mo-S phase, *J. Catal.* **68**, 433.

61 Delmon B. (1979) A new mechanistic model explaining synergy in hydro-treatment catalysts. *C.R. Acad. Sci.* series C **289**, 173.

62 Delmon B. (1979) A new hypothesis explaining synergy between two phases in heterogeneous catalysis the case of hydrodesulfurization catalysts. *Bull. Soc. Chim. Belg.* **88**, 979.

63 Delmon B. (1980) A new concept explaining catalytic synergy between two solid phases, *React. Kinet. Catal. Lett* **13**, 203.

64 Wivel C., Candia R., Clausen B.S., Morup S., Topsøe H. (1981) On the catalytic significance of a CoMoS phase in $CoMo/Al_2O_3$ hydrodesulfurization catalysts: Combined in situ Mössbauer emission spectroscopy and activity studies, *J. Catal.* **68**, 453.

65 Van der Meer Y., Vissenberg M.J., De Beer V.H.J., Van Veen J.A.R., Van Der Kraan A.M. (2002) Characterization of carbon and alumina-supported NiW and CoW sulfided catalysts, *Hyp. Interact.* **139**, 51.

66 Breysse M., Bachelier J., Bonnelle J.P., Cattenot M., Cornet D., Decamp T., Duchet J.C., Engelhard P., Frety R., Gachet C., Geneste P., Grimblot J., Gueguen C., Kasztelan S., Lacroix M., Lavalley J.C., Leclercq C., Moreau C., De Mourgues L., Olive J.L., Payen E., Portefaix J.L., Toulhoat H., Vrinat M. (1987) New developments in hydrotreating catalysis: characterization and optimization of $NiW/A1_2O_3$ catalysts, *Bull. Soc. Chim. Belg.* **96**, 829.

67 Clausen B.S., Morup S., Topsøe H., Candia R. (1976) *J. Phys. Colloq.* **37**, C6–249.

68 Karroua M., Grange P., Delmon B. (1989) Existence of synergy between "CoMoS" and Co_9S_8, new proof of remote control in hydrodesulfurization, *Appl. Catal.* **50**, 5–10.

69 Passaretti J.D., Chianelli R.R., Wold A., Dwight K., Covino J. (1986) Preparation and properties of the systems $Co_{1-x}Rh_xS_2$, $Co_{1-x}Ru_xS_2$, and $Rh_{1-x}Ru_xS_2$, *J. Solid State Chem.* **64**, 365.

70 McCarty K.F., Anderegg J.W., Schrader G.L. (1985) Hydrodesulfurization catalysis by Chevrel phase compounds, *J. Catal.* **93**, 375.

71 Rao CNR (1993), in: *Proceedings 3rd International Conference on Advanced Materials, Tokio.*

72 Hirschon A.S., Wilson R.B., Laine R.M. (1987) Ruthenium promoted hydrodenitrogenation catalysts, *Appl. Catal.* **34**, 311.

73 Prada Silvy R. Hydrogenation of aromatic compounds in Diesel fuel over NiWPd/TiO2-Al_2O_3 catalysts, *Oil Gas Sci. Technol. - Rev. IFP Energies nouvelles*. Article in preparation.